NASA/GRC Contract No. C-7076-N

UES Project No. 707

Designing Gamma TiAl Alloys (K5 Based) for Use at 840°C and Above

Young-Won Kim and Sang-Lan Kim
UES, Inc.
4401 Dayton-Xenia Road
Dayton, OH 45432
Phone: 937-255-1321
Email: young-won.kim@wpafb.af.iml

Final Report for Period: 08 February - 31 May 2002

(7 June 2002)

Public Distribution (Recommended)

Acknowledgment

The program was originally formulated by Dr. Paul Bartolotta of Glenn Research Center at Lewis Field, and has been managed by Dr. J. Daniel Whittenberger of GRC. The authors gratefully acknowledge their support and guidance. In particular, Dr. Whittenberger has contributed to this program significantly through technical discussions and suggestions, and also testing/evaluating selected materials generated from this program. Most of the experiments have been carried out at Air Force Research Laboratory (AFRL) Materials & Manufacturing Directorate (MMD). The authors would like to thank AFRL/MMD for kindly allowing us to use their experimental facilities.

Table of Contents

0.0 Proposal Description

Objective: The program is aimed to develop microstructural forms in a K5-based alloy that can be used for thin sheet as well as rotational components that can be used at temperatures equal to, or higher than, 840°C. The wrought ingot-metallurgy-processing route involving forging will be employed to generate the application-specific microstructural forms, and their properties will be validated by testing tensile and creep properties and optional oxidation resistance measurements.

Statement of Work: The task is to generate optimum microstructures in K5 based alloys and evaluate the mechanical properties for critical applications. Alloys shall be selected on the basis of K5 alloy composition, and alloy ingots shall be produced through melting, HIP'ing, and forging. Phase transition temperatures and the composition shall be determined as the base information for microstructure control. Microstructures to be evaluated shall include fully-lamellar microstructures, duplex material and nearly-lamellar microstructures in forged material. Aging experiments at high temperatures and high-magnification microscopic analyses will be carried out to define the size distribution of carbide as a function of aging temperature/time. The contractor will then define optimum materials' conditions by evaluating the mechanical behavior including tensile and creep properties tested on some selected microstructures. An effort will be made in determining the maximum useful temperature limit for each microstructure type under given stress conditions. Because of the limited funding for the proposed task, it is recommended that more engineering-related creep testing be conducted by GRC for the selected material conditions. As needed, the contractor shall provide GRC with tensile creep test specimens having suitable microstructures. Evaluation of the cyclic oxidation resistance is recommended.

Proposed Technical Approach: The proposed work will be carried out through four interrelated tasks that are to optimize the microstructures in wrought-processed material of K5 based alloys that will generate adequate creep resistance for specific applications. Alloys will be selected within the composition range of alloy K5, and typical microstructures will be developed/evaluated by annealing the forged material for each of three microstructural classes, that is, fully-lamellar (FL) microstructures, duplex (DP) material and nearly-lamellar (NL) microstructures. Aging experiments will be conducted on a selected material for each class, and high-magnification microscopic analyses will be performed to define the size distribution of carbide as a function of aging temperature/time. The optimum material's

conditions will be defined by conducting property testing on the materials in selected annealing /aging conditions.

1.0 Material Preparation

1.1 Alloy Selection

Three candidate alloys selected for the program include:

(1) 01A: Ti-46Al-1.5Cr-3.0Nb-0.2W-0.2B-0.2C (Nominal)
(2) 01B: Ti-46Al-1.5Cr-3.0Nb-0.3W-0.2B-0.35C (Nomnal)
(3) 01C: Ti-46Al-1Cr-3.0Nb-0.2W-0.2B-0.2C-0.15Si (Nominal)

The selected compositions (all in at%) are modified slightly from the original K5 (Ti-46.5Al-2Cr-3Nb-0.2W-0.2B-0.2C) in an effort to enhance the oxidation resistance (decrease in Cr and increase in W) and improve creep resistance (increase in C and introduction of Si). A small decrease in Al content (from 46.2 to 46.0) was to insure adequate strength levels. It is known that controlling the Al content is the most difficult in producing gamma alloy ingots, and that within the Ti- (45-47)Al range, the yield strength is reduced by roughly 180MPa for every 1at% loss of Al content. Unlike alloy 99B, which was selected/investigated for the last GRC contract (C-7076-K), these alloys do not contain Mn, Zr, and Hf. The removal of these alloying elements was made because the original expectation for improved creep resistance was not realized in ally 99B. The simplified composition is also expected to improve the ductility and hot-workability. A decrease in Al content (from 46.5 to 46.0) was to insure adequate strength levels. It is known that controlling the Al content is the most difficult in producing gamma alloy ingots, and within the Ti-(44-47)Al range, the author has previously analyzed that the yield stress of gamma alloys is reduced by roughly 180MPa for every 1at% decrease of Al content.

In the beginning of the contract period, forged material of alloy K5A (later on called as 01D) was evaluated for microstructure evolution and control while the three selected alloys were produced. An alloy K5A ingot was produced and forged toward the end of the last GRC contract in an anticipation of expected delay in the material preparation. The nominal composition of thi exploratory alloy, was:

(4) 01D (also called as K5A): Ti-45.5Al-1.5Cr-3Nb-0.2W-0.2B-0.2C (Nominal)

1.2 Ingot Production and Chemistry

A 4" diameter and 14 to 18" long ISM ingot for each of alloys - 01A, 01B, and 01C - was produced at FlowServe, Dayton, using the induction skull melting (ISM) technique (March 28, 2001) and HIP'ed at Howmet at 1300°C and 207 MPa for 6h to remove shrinkage porosity (April 20, 2001). Alloy 01D (K5A) ISM ingot having the same size was produced in collaboration with FlowServe just before the current contract, as described later. The wet chemical analysis showed that the actual compositions are different from the nominal, shown below.

01A: Ti-47.0Al-1.7Cr-3.0Nb-0.20W-0.18B-0.23C-0.2Ox
01B Ti-45.6Al-1.5Cr-3.1Nb-0.31W-0.15B-0.43C-0.19Ox
01C: Ti-45.7Al-1Cr-3.0Nb-0.30W-0.18B-0.40C-0.2Si-0.23Ox
01D: Ti-44.7Al-1.7Cr-3Nb-0.2W-0.2B-0.3C **(=K5A)**

As expected, there are variations of Al content, -0.7 to +0.5 at%. Carbon contents are generally higher than the nominal, while the boron contents are slightly lower. DTA measurements were conducted on forged material, and the results were analyzed to determine the alpha transus (Tα) for each alloy forging, as shown below.:

Alloy	Alpha Transus (Tα)
01A	1356°C
01B	1309°C
01C	1311°C
01D (K5A)	1288°C

1.2 Forging

One billet having 10.1-cm diameter and 20.2-cm length was machined from each alloy ingot and forged at Wyman-Gordon Forging, Houston, Texas. The billets were isothermally forged at 1150°C to 1.82-cm thick plates (91% reduction) through a two-step forging procedure involving an intermediate annealing step. A constant forging ram speed was employed, which corresponded to the initial strain rate of about 0.001/sec. Subsequent strain rates,

which constantly increase as the billet thickness is reduced, were expected to be4effective in breaking up of the cast structures.

2.0 Microstructure Evolution and Control

Coupon specimens, sectioned from alloy forging plates, were given annealing treatments in an air furnace at pre-selected temperatures below and above the respective alpha transus. Subsequent cooling was done by direct air cooling (AC) to RT, or by furnace cooling (FC) to an intermediate temperature and then AC to RT. The resulting microstructures were characterized/evaluated by various microscopy (PL, SEM, BEI and TEM), microprobe composition analysis, X-ray dot mapping and Rockwell C hardness (RcH) measurements.

2.1 Alloy 01D (K5A): Microstructure Evolution

Microstructures evolved in alloy K5 forging was investigated in the samples given the following heat treatments:

K5A-001:	1320°C/1h/AC	K5A-004:	1280°C/1h/AC
K5A-002:	1300°C/1h/AC	K5A-005:	1270°C/1h/AC
K5A-003:	1290°C/1h/AC	K5A-006:	1240°C/1h/AC

As reported in the 1st progress report, the preparation of alloy ingots takes up to four months. Since this delay was anticipated, early on (November 2000 through February 2001) we prepared alloy K5A, in collaboration with Flowserve and Wyman-Gordon. Preliminary characterization on K5A forging, had been conducted while the three alloys (01A, B, and C) were being processed. In spite of the unexpected low Al content, the alloy showed very interesting, potentially important results to the future alloy modification. Annealing treatments were conducted at temperatures above and below the alpha transus (1288°C), followed by air cooling to RT, and some of the resulting microstructures are shown in Fig. 2.1. Clearly, fully-lamellar (FL) microstructures are generated at higher temperatures, a nearly FL (NFL; K5A -004) and a nearly lamellar (NL) (K5A-006) are produced at lower temperatures. Interestingly, the FL grain size appears to be finer at higher temperatures (K5A-001 vs. K5A-002), with an attractively fine size of about 100 μm for K5A-001. The NFL microstructure (K5A-004) is a mixture of fine gamma grains (<10 μm), Fig. 2.2, and fine lamellar grains (an average of about 30 μm). This mixture combination is expected to yield potentially important

properties for sheet applications, that is high strength, good ductility (resulting from the presence of scattered fine duplex grains), and excellent fatigue properties. Improved creep resistance over the duplex material is expected because of remarkably fine lamellar spacing present in the lamellar grains, Fig. 2.2.

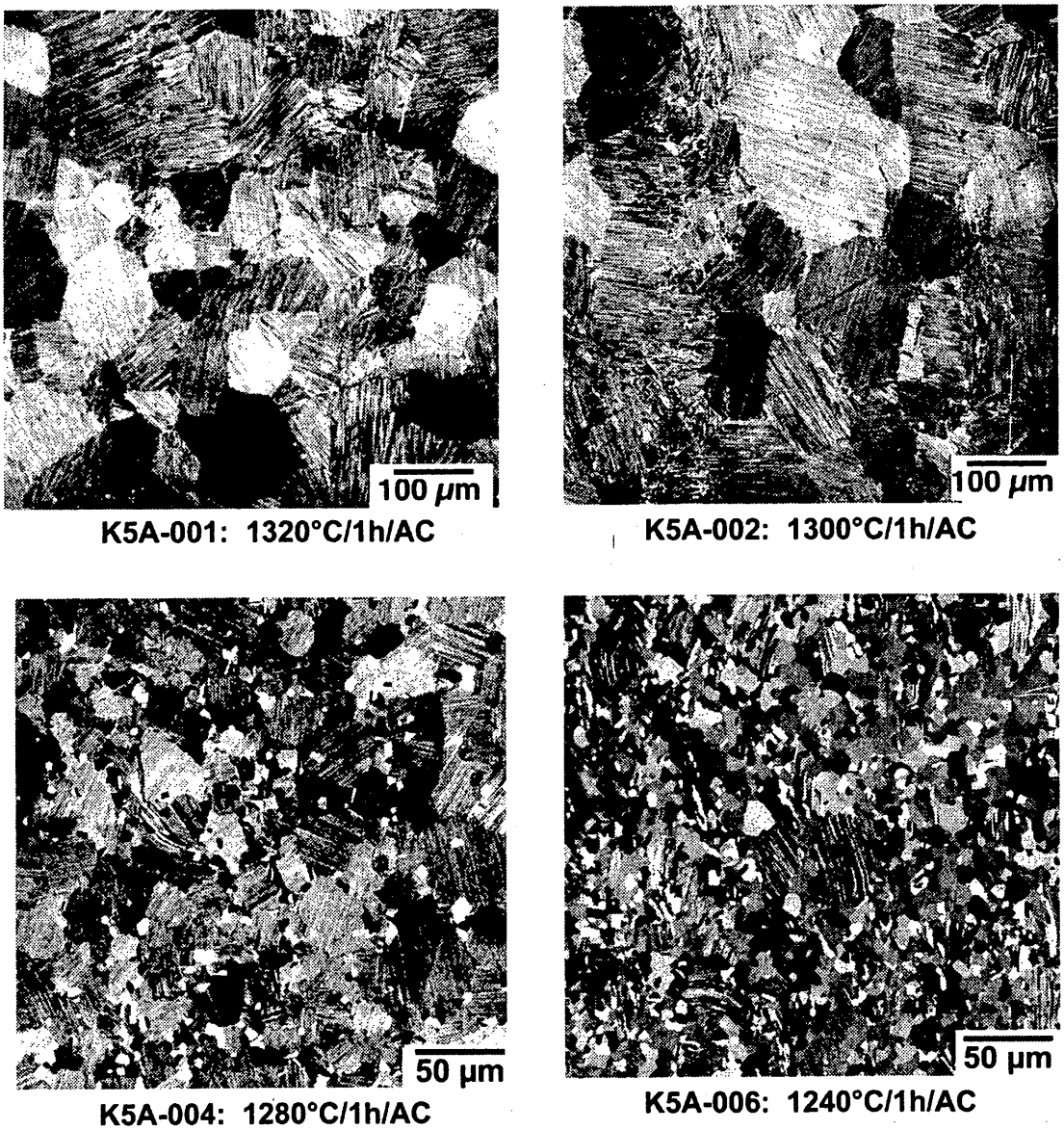

Fig. 2.1. Effect of annealing temperature on the microstructure (under polarized light) developed in forged 01D (K5) alloy material that was air-cooled to RT after the annealing for 1h. The alpha transus temperature was determined to be 1288°C according to the DTA analysis.

Remarkable strength levels are achieved with the above microstructures, shown in Fig. 2.3, where the hardness measured using the Rockwell C (Rc) indent is plotted against annealing temperature. The yield strength (YS) values were derived from the Rc-YS relationship B in Fig. 2.4a, which have been generated from the measurements on various gamma alloys including K5 alloys at Wright-Patterson. Overall, the strength levels are extraordinary, exceeding 1000MPa for FL materials. In spite of the relatively coarser grain sizes, YS increases as the volume fraction of lamellar grains increase, but it remains constant for FL material regardless of annealing temperature. This may be explained in terms of alpha-2 volume fraction and the lamellar spacing effect; however, this explanation has yet to be quantified. Yet, this result will be an important consideration for generating engineering microstructures for the future program.

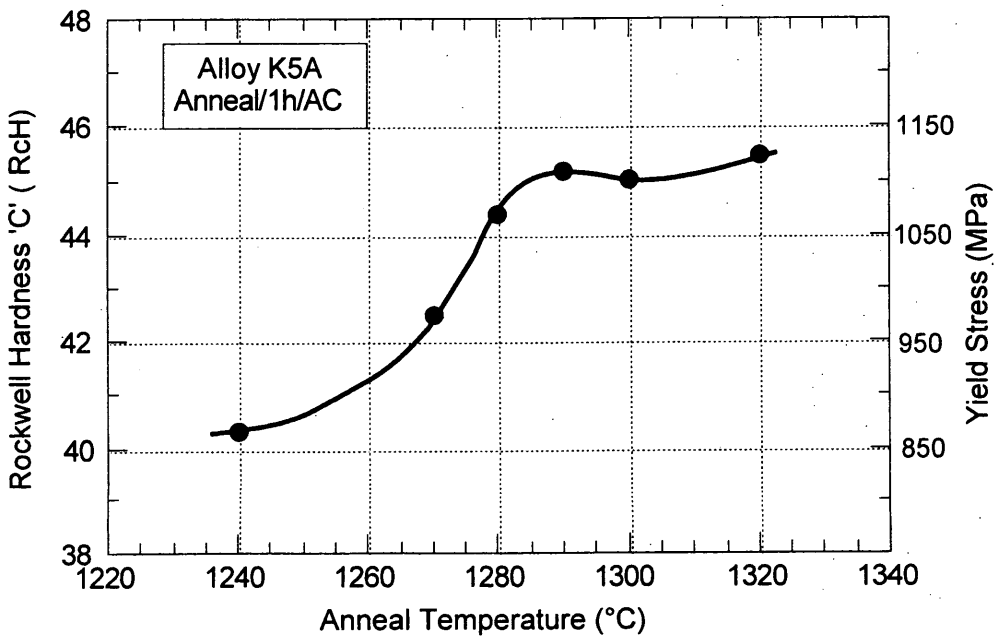

Fig. 2.3: Effect of annealing temperature on the Rockwell 'C' hardness values and the corresponding yield strength variations in alloy 01D (K5A). The annealing treatment consisted of holding 1 hr followed by air cooling (AC) to RT.

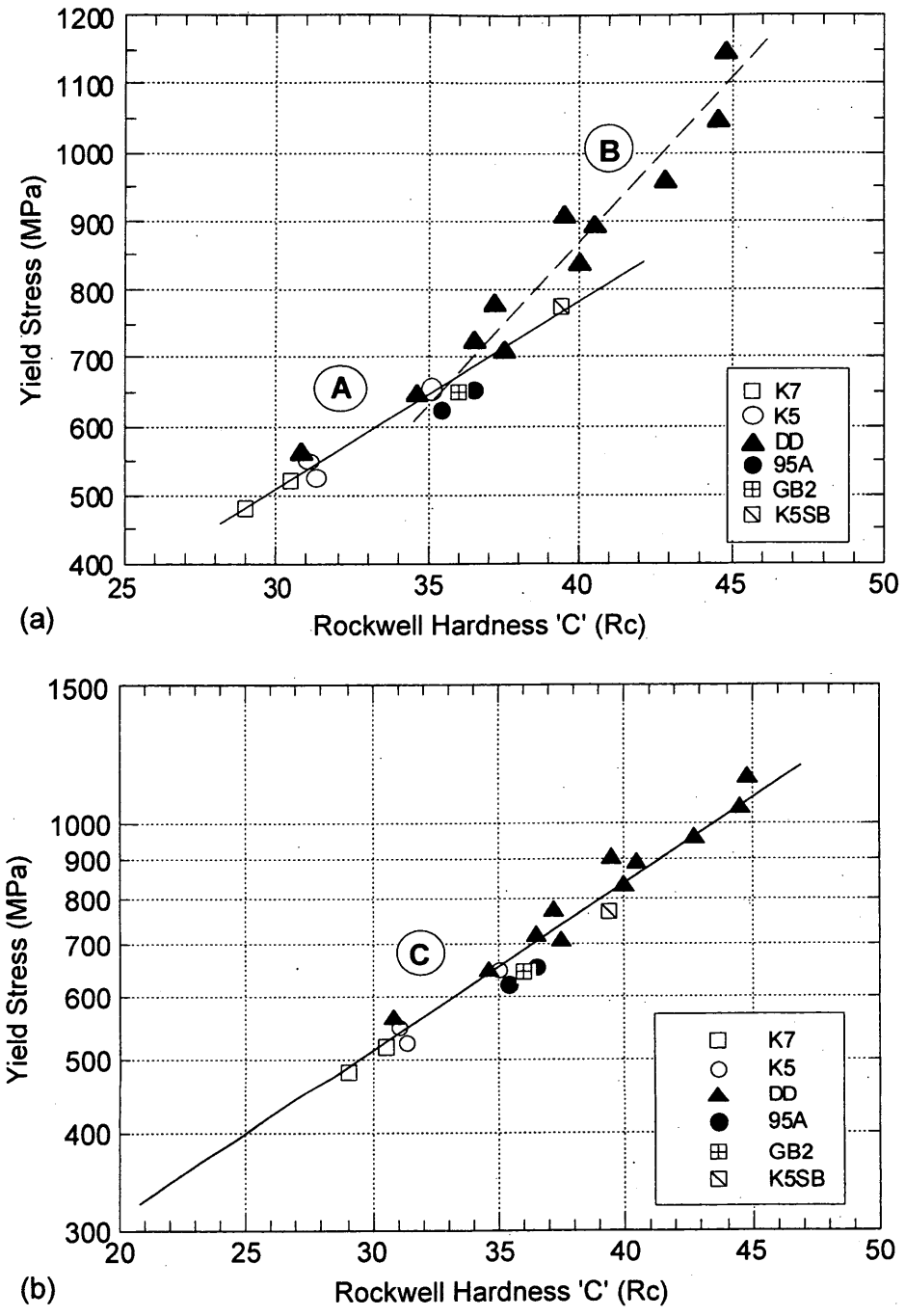

Fig. 2.4: Yield strengths of various gamma TiAl alloys in fully-lamellar forms are plotted against their Rockwell 'C' hardness values. Their relationships can be represented by grouping them into two linearly-related regimes (A and B); with regime A for lower strength levels and regime B for higher strength levels (a). A better relationship for the entire hardness range (C) can be formulated in the linear-log space (b)

Alloy K5A coupon samples were annealed at temperatures in the alpha- phase field followed by furnace cooling (FC) to an intermediate temperature (between 1300°C and 700°C) and then immediately air cooled to RT. The average FC rate was roughly 60°C/min from 1330°C and 1100°C. The conditions are specified below.

K5A-062: 1330°C/2h / FC*/ 1300°C/AC
K5A-060: 1330°C/2h / FC*/ 1250°C/AC
K5A-030: 1320°C/2h / FC*/ 1250°C/AC
K5A-031: 1320°C/2h / FC*/ 1200°C/AC
K5A-032: 1320°C/2h / FC*/ 1100°C/AC
K5A-033: 1320°C/2h / FC*/ 1000°C/AC
K5A-034: 1320°C/2h / FC*/ 900°C/AC
K5A-035: 1320°C/2h / FC*/ 700°C/AC

The resulting hardness variations and corresponding yield strength levels are plotted in Fig. 2.5 as a higher cooling temperature, as exemplified for K5A-031 and K5A-034 in Fig. 2.6. It is noted that increases in cooling temperature increase the effective cooling rate for lamellar formation. The strength decreases rapidly, with decreases of cooling temperature in the range between 1250°C and 1100°C, to a plateau value of RcH~35.7 for lower cooling temperatures, Fig. 2.5.

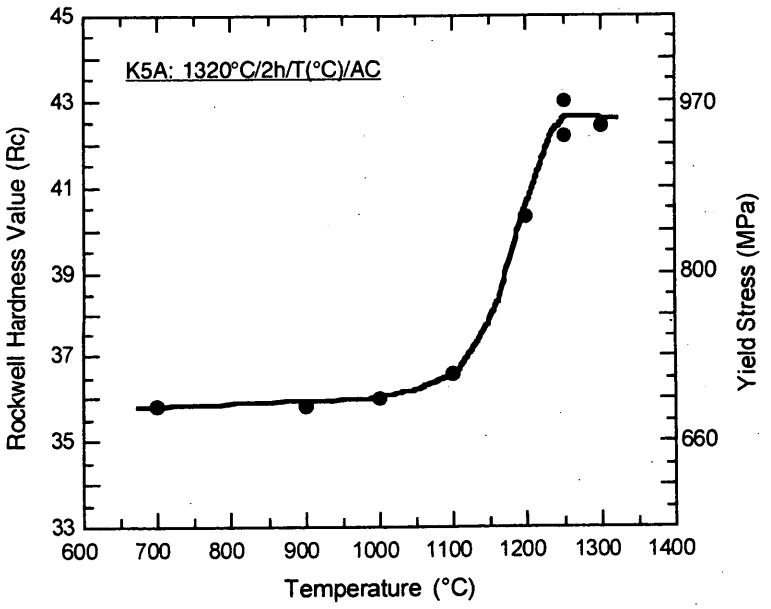

Fig. 2.5: Hardness variation against cooling temperature in alloy K5A forging that was alpha annealed, furnace cooled to an intermediate temperature, and then immediately air-cooled. The corresponding yield strength range is also shown.

2.2 Alloys 01A, 01B and 01C: Microstructure Evolution

Number of temperatures were selected for annealing these alloys forgings. The treatments consisted of holding for 2-4 h at the selected annealing temperature and then FC (60°C/min) to a fixed cooling temperature of 1200°C, followed by AC to RT. These are listed below.

Heat Treatment (Annnealing + Cooling) Conditions for 01A, 01B and 01C Alloys

01A-001:	1270°C/4h/FC/1200°C/AC	01A-002:	1290°C/4h/FC/1200°C/AC
01B-001:	1270°C/4h/FC/1200°C/AC	01B-002:	1290°C/4h/FC/1200°C/AC
01C-001:	1270°C/4h/FC/1200°C/AC	01C-002:	1290°C/4h/FC/1200°C/AC
01A-003:	1310°C/2h/FC/1200°C/AC	01A-004:	1330°C/2h/FC/1200°C/AC
01B-003:	1310°C/2h/FC/1200°C/AC	01B-004:	1330°C/2h/FC/1200°C/AC
01C-003:	1310°C/2h/FC/1200°C/AC	01C-004:	1330°C/2h/FC/1200°C/AC
01A-005:	1350°C/2h/FC/1200°C/AC	01A-006:	1370°C/2h/FC/1200°C/AC
01B-005:	1350°C/2h/FC/1200°C/AC	01B-006:	1370°C/2h/FC/1200°C/AC
01C-005:	1350°C/2h/FC/1200°C/AC	01C-006:	1370°C/2h/FC/1200°C/AC

The resulting Rockwell hardness values are plotted against annealing temperature in Fig. 2.7, where the alpha transus for each alloy is indicated by an arrow. Corresponding YS values, which were estimated from the relation C in Fig. 2.4, are also shown in Fig. 2.7. Unlike the case for alloy K5A (Fig. 2.3), 01B and 01C alloys materials show respective peaks in hardness, that occur after annealing at about $T\alpha$ + 20°C. 01C alloy material shows slightly higher strength levels than 01B material for all annealing temperatures. Alloy 01A having a higher alpha transus also tends to show increased hardening at temperatures slightly higher than the transus. The relatively lower strength levels shown in 01A material are simply because of the lower Al content. The results clearly indicate that the Al content should be 46at% or lower if the RT YS greater than 650 MPa is required in forged/annealed material.

Three types of typical microstructures (duplex, NL, and FL) were produced by the annealing treatments, and some of the typical microstructures produced by the annealing are shown in Figs. 2.8, 2.9 and 2.10. Fig. 2.8 shows a typical duplex microstructure, having very fine grains (average of ~8 μm), produced in all alloys upon annealing at T=$T\alpha$-20°C. Fig. 2.9 shows microstructures generated in the three alloys in a treatment condition, 1320°C/2h/FC/1200°C/AC (designated as 01X-005). As expected, 01A-005 material shows a NFL microstructure, and 01B-005 and 01C-005 have FL microstructures. Though not

quantified, the lamellar spacing of the 01C FL material is apparently finer that of the 01B FL material. This is reflected in the higher strength for 01C shown in Fig. 2.7. Nevertheless, the grain sizes for these two alloys appear to be similar, which is a reflection of similar amounts of boron and Al contents in both alloys. The grain and lamellar morphologies in the 01C-005 material are shown under the back-scattered electron imaging condition, Fig. 2.10, exhibiting continuous but unevenly thick alpha-2 plates (imaged bright) that are sandwiched by unevenly thicker gamma plates (imaged dark).

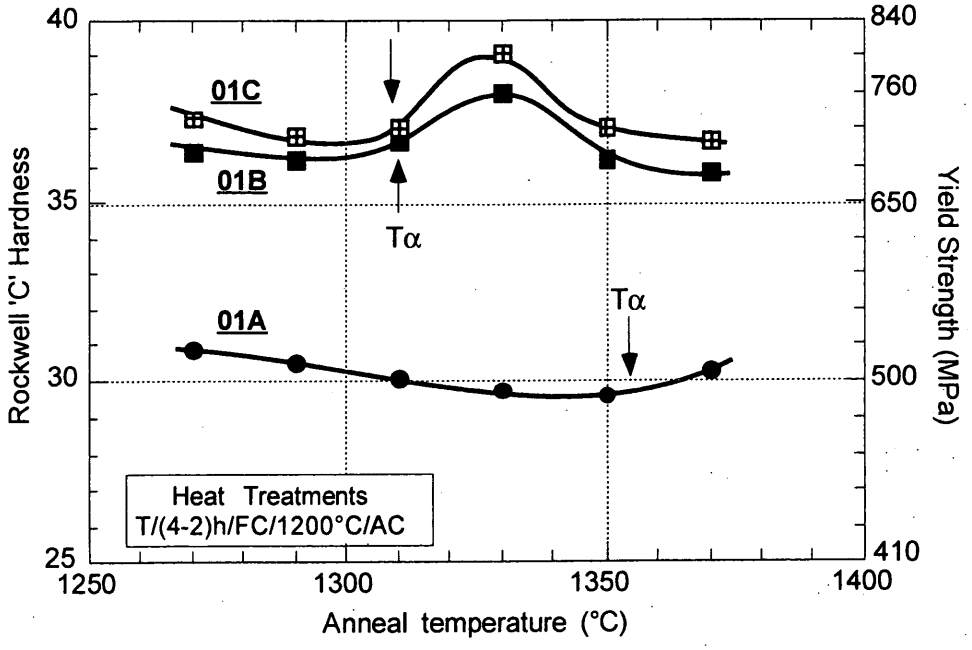

Fig. 2.7: Effect of annealing temperature on the Rockwell 'C' hardness values and the corresponding yield strength variations in alloys 01A, 01B and 01C. The heat treatment consisted of annealing for 2-4 hrs, followed by cooling to 1200°C at a furnace cooling rate (~60°C/min) and then air cooling to RT.

K5A-004: 1280°C/1h/AC

Fig. 2. 2 Back-scattered electron (BSE) image of the nearly lamellar (NL) Microstructure (K5A-004) shown in Micrograph 1. The NL microstructure consists of a small volume fraction of fine (2-10 µm) gamma grains (imaged dark) mostly present along the boundaries of lamellar grains having an average size of 18 µm. For most of lamellar grains, the lamellar spacing is too fine for the laths to be resolved clearly in the micrograph.

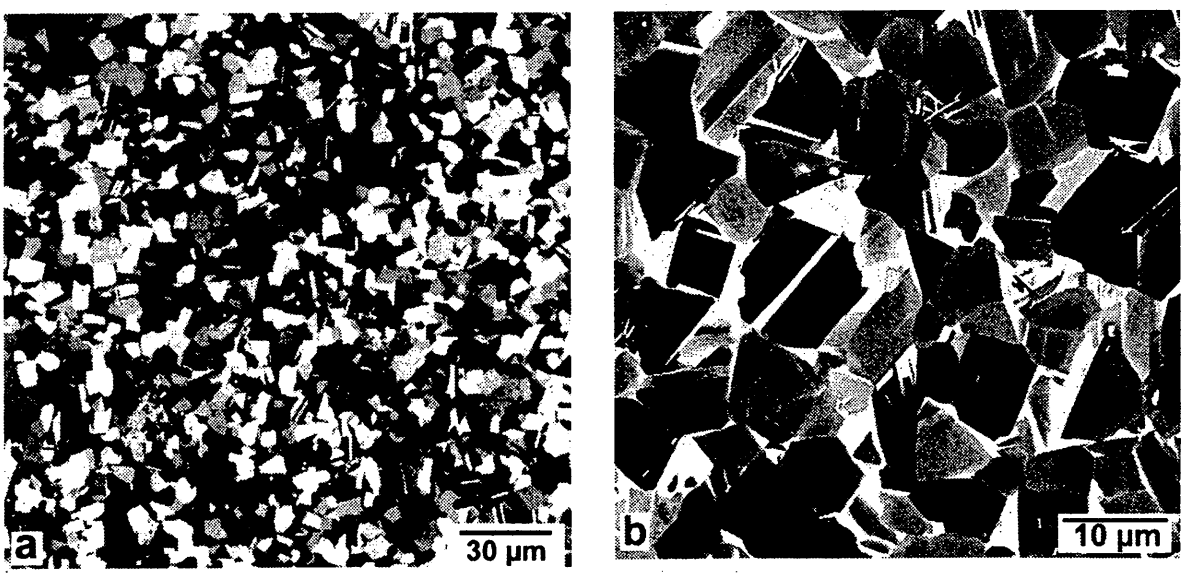

Fig. 2.8: Typical duplex microstructure of alloys - 01A , 01B and 01C - under polarized light (a) and back-scattered imaging (b) conditions. The microstructures were produced after annealing at temperatures in the two-phase field (alpha and gamma) about 20°C below the alpha transus of each alloy (01A-004, 01B-002, and 01C-002).

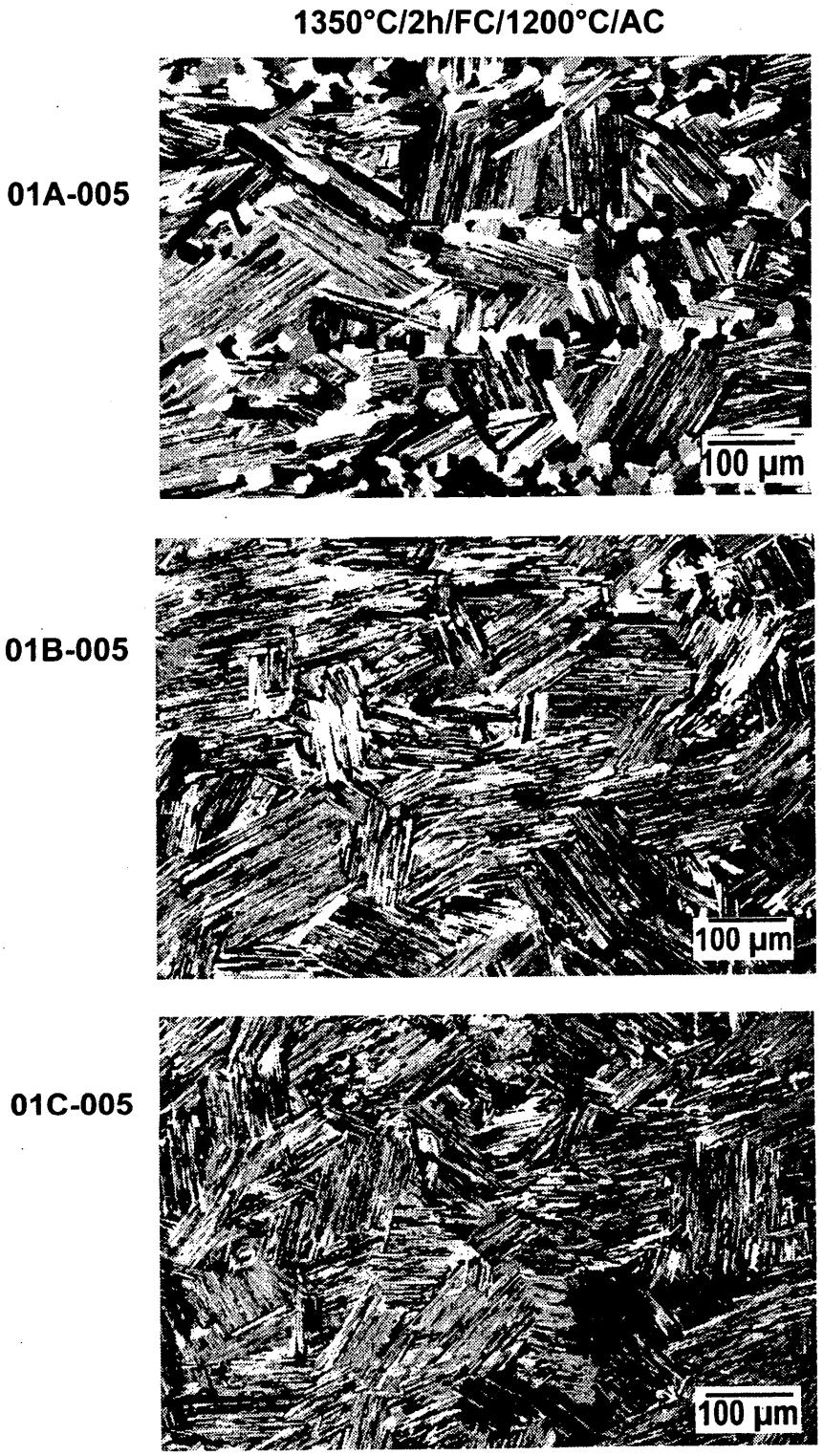

Fig. 2.9: Microstructures of the three wrought alloys produced by annealing at 1350°C for 2h and then furnace cooling (60°C/min) to 1200°C followed by air-cooling to RT (01X-005). In this heat treatment condition, alloy 01A shows a nearly lamellar (NL) microstructure (01A-005) and both 01B and 01C alloys show fully-lamellar (FL) microstructures (01B-005 and 01C-005).

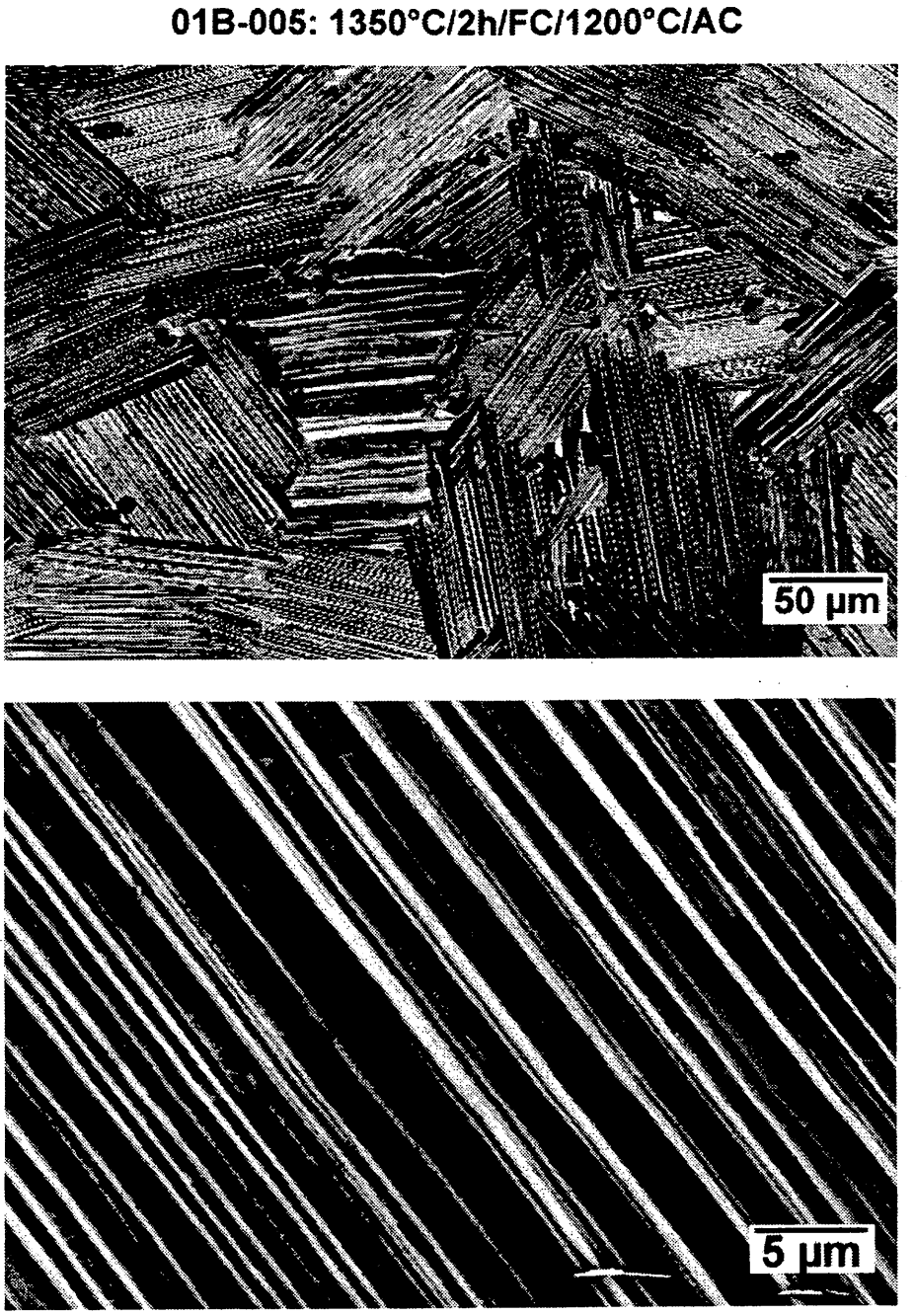

Fig. 2.10: Back-scattered electron images of the 01B-005 FL microstructure at two different magnifications showing lamellar grains (occasionally containing curved, coarse laths) and a typical, continuous, well-defined lamellar arrangement present within a grain.

3.0 Engineering Microstructures

Extensive aging experiments were conducted on FL material to investigate thermal instability of lamellar structures that occurs during aging treatments. FL material was generated in various annealing and cooling conditions.

3.1 01D (K5A): Aging Responses

Various aging conditions employed on 01D FL materials are listed below.

K5A-020: 1320°C/2h/FC/1100°C/AC
K5A-021: K5A-020 + 900°C/6h/AC
K5A-022: K5A-020 + 900°C/18h/AC
K5A-023: K5A-020 + 900°C/48h/AC
K5A-024: K5A-020 + 900°C/96h/AC
K5A-025: K5A-020 + 900°C/192h/AC

K5A-031: Anneal (1320°C/2h /FC/1200°C/AC)
K5A-041: K5A-031 + 900°C/24h/AC
K5A-042: K5A-031 + 900°C/72h/AC
K5A-043: K5A-031 + 900°C/168h/AC
K5A-044: K5A-031 + 900°C/336h/AC
K5A-051: K5A-031 + 1000°C/24h/AC
K5A-052: K5A-031 + 1000°C/72h/AC
K5A-053: K5A-031 + 1000°C/168h/AC
K5A-054: K5A-031 + 1000°C/336h/AC

K5A-060: 1330°C/2h/FC/1250°C/AC
K5A-061: 1330°C/2h/FC/1250°C/AC + 900°C/48h/AC
K5A-062: 1330°C/2h/FC/1300°C/AC
K5A-063: 1330°C/2h/FC/1300°C/AC + 900°C/48h/AC

K5A-090: 1320°C/2h/FC/1280°C/AC + 800°C/48h/AC
K5A-091: 1320°C/2h/FC/1280°C/AC + 800°C/192h/AC
K5A-092: 1320°C/2h/FC/1280°C/AC + 900°C/72h/AC

A modified FL microstructure was generated by annealing specimens under a fixed condition (K5A-020), and then they were aged isothermally at 900°C up to 192h. The annealing condition (K5A-20) was 1320°C/1h/CR (50°C/min)/1100°C/AC, and this condition was selected to reduce the (too high) strength levels realistically and to utilize practical cooling conditions. The Rockwell hardness values for the resulting microstructures are plotted against aging time in Fig. 3.1, where YS values estimated using the relation B in Plot 3a are also shown. Similar but a better estimation of the YS from the Rc-YS relationships can be made more globally from the

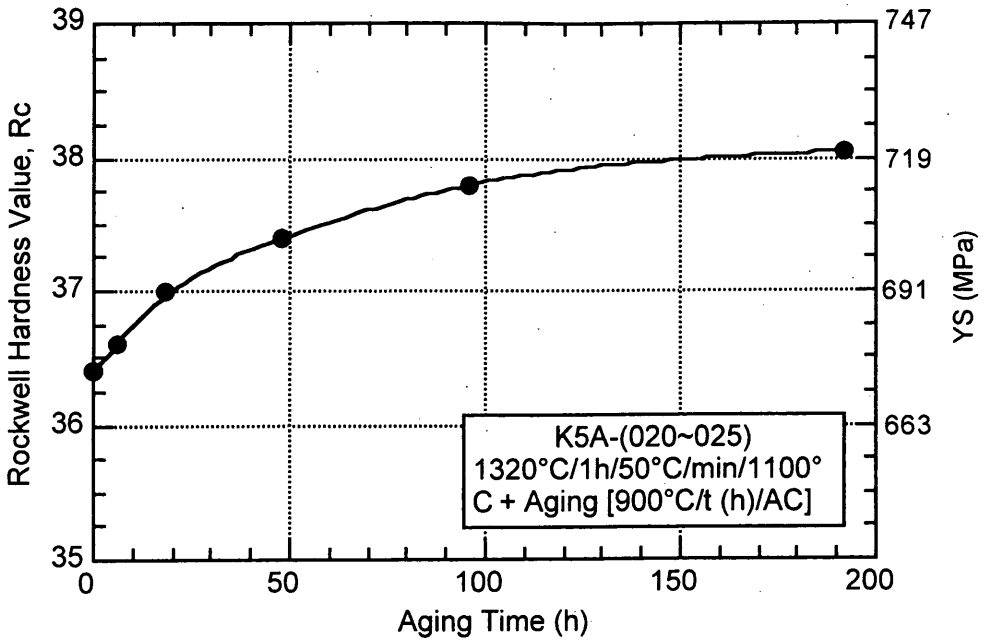

Fig. 3.1: Effect of aging on hardness variation in 01D (K5A) in a fully-lamellar microstructure form, showing the hardness constantly increasing with aging. Corresponding YS levels are also indicated.

relation C in established in the linear Rc - log YS field, shown in Fig. 2.4. Clearly, the alloy K5A shows a gradual but distinct age-hardening phenomenon that is different from the typical one with a definite peak strength. Some of the resulting microstructures are shown under polarized-light condition in Fig. 3.2. As shown, no definite changes are obvious with aging at 900°C for up to 192h. Therefore, what causes the hardening is unclear, but some speculations can be made by evaluating the microstructures at higher magnifications shown in Figs. 3.3 to 3.7. As aging proceeds, the well-defined lath structures (alternating gamma and alpha-2 plates) produced by the specified annealing treatment become gradually unstable and eventually broken into particles to form particle arrays which replace the alpha-2 plate. This equilibration process, however, does not appear to be complete even after 192h at 900°C as is clear in Fig. 3.6. Generally, the broken-up alpha-2 particles appear in two different morphologies that are elliptical Fig. 3.6b and needle-shaped (Figs. 3.4, 3.5c, and 3.6c). The needle-shaped alpha-breakups are always observed in coarse (often-curved) lamellar arrangements. Though not clearly demonstrated, there appears to be certain habit directions for these breakups, Fig. 3.6c. It can be visualized that two adjacent gamma plates now share a sandwiched alpha-2 particle arrangement instead of a perfect alpha-2 foil.

Other important features observed during aging include variations in grain boundary morphology and lamellar spacing. Though not quantified yet, slight increases in lamellar spacing appear to have taken place upon aging which reduces the volume fraction of the alpha-2 plates. In some cases alpha-2 plates disappear completely, or at least partially, (see Figs. 3.5b and 3.6c), which effectively thickens the gamma plates, provided the adjacent gamma plates have the same orientation. The aging process yield gamma grains along the lamellar grains as the result of apparent recrystallization, often resulting in lamellar grains almost completely isolated from each others after 192 h, as shown in Fig.3.6a.

From the above described observations/analysis of microstructural changes occurring during aging, the measured age-hardening may be qualitatively explained in terms of increased strength due to the breaking up of alpha-2 plates. It is known that the reduction in alpha-2 volume fraction results in the production of fine carbides (Ti2AlC) as well as some beta particles. The net results are that the broken particles are a mixture of alpha-2, beta and carbide particles. Most of these particles occupy the gamma-gamma interfaces (which are near, and parallel to, the easy deformation direction), making deformation difficult. This increased resistance to deformation is apparently greater than the possible reduction by a (possibly) increased lamellar spacing and the presence of recrystallized gamma grains along the lamellar GB. This aspect will be investigated/analyzed in more detail during the third reporting period. It will be also interesting to see if the increased RT strengthening by aging would increase creep resistance which GB gamma grains may influence detrimentally.

The hardness values measured and corresponding yield strength levels are plotted against aging time for both temperatures in Fig. 3.7. Unlike alloy 01B and 01C materials (see Fig. 3.12), the yield strengths increased for both aging temperatures initially, and were greater for 900°C aging than at 1000°C. The YS levels at 900°C remained at least the same as the unaged value all the time, while the levels decreased below the unaged value when aged longer than 100h. It is noted that the YS levels are greater than 700 MPa even after 350h at 1000°. Aging at 900°C and 1000°C resulted in the breaking-up of alpha-2 plates and the formation of carbides, typically in stringer forms. A typical example for 900°C aging is shown in Fig. 3.8A. At 1000°C, the same process takes place; however, gamma grains are recrystallized and grow along FL grain boundaries and even in the grain interior, when aging time is longer than 72h, Fig. 3.8B. This process is expected to reduce the creep resistance.

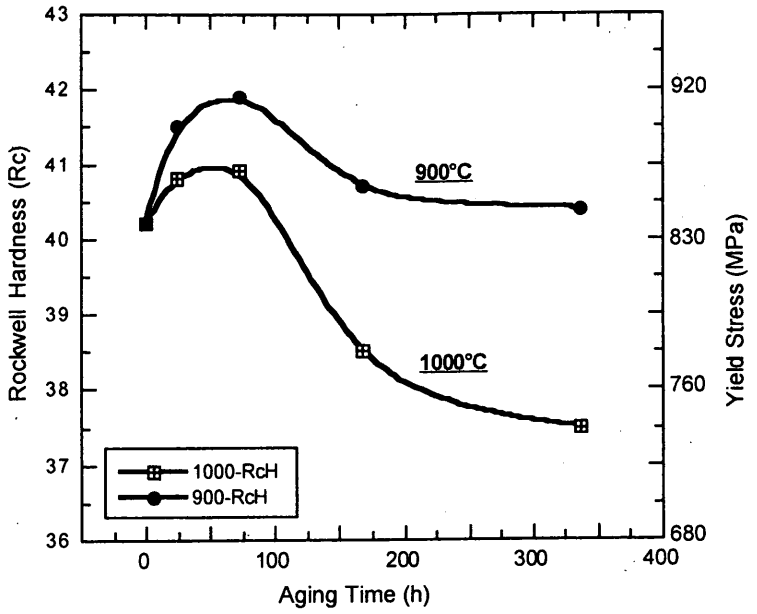

Fig. 3.7: Variations of Rockwell C hardness and yield strength of 01D (K5A) in FL forms against aging time at 900°C and 1000°

3.2 01B and 01C: Aging Response

Various aging treatments were conducted on 01A, B and C alloy samples, as listed blow.

01A-011: 01A-001 (1270°C/4h/FC/1200°C/AC) + 900°C/48h/AC
01B-011: 01B-001 (1270°C/4h/FC/1200°C/AC) + 900°C/48h/AC
01C-011: 01C-001 (1270°C/4h/FC/1200°C/AC) + 900°C/48h/AC

01A-012: 01A-003 (1310°C/2h/FC/1200°C/AC) + 900°C/48h/AC
01B-012: 01B-003 (1350°C/2h/FC/1200°C/AC) + 900°C/48h/AC
01C-012: 01C-003 (1310°C/2h/FC/1200°C/AC) + 900°C/48h/AC

01A-013: 1360°C/2h/FC/1200°C/AC + 900°C/48h/AC
01B-013: 1360°C/2h/FC/1200°C/AC + 900°C/48h/AC
01C-013: 1360°C/2h/FC/1200°C/AC + 900°C/48h/AC

01B-040: SRT (1000°C/3h/FC/RT) + Anneal (1370°C/2h/FC/1200°C/AC)
01C-040: SRT (1000°C/3h/FC/RT) + Anneal (1370°C/2h/FC/1200°C/AC)

01B-041: 01B-040 + 900°C/5h/AC
01B-042: 01B-040 + 900°C/24h/AC
01B-043: 01B-040 + 900°C/48h/AC
01B-044: 01B-040 + 900°C/96h/AC
01B-045: 01B-040 + 900°C/192h/AC

01C-041: 01C-040 + 900°C/5h/AC
01C-042: 01C-040 + 900°C/24h/AC
01C-043: 01C-040 + 900°C/48h/AC
01C-044: 01C-040 + 900°C/96h/AC
01C-045: 01C-040 + 900°C/192h/AC

01B-051: 01B-040 + 1000°C/5h/AC
01B-052: 01B-040 + 1000°C/24h/AC
01B-053: 01B-040 + 1000°C/48h/AC
01B-054: 01B-040 + 1000°C/96h/AC
01B-055: 01B-040 + 1000°C/192h/AC

01C-051: 01C-040 + 1000°C/5h/AC
01C-052: 01C-040 + 1000°C/24h/AC
01C-053: 01C-040 + 1000°C/48h/AC
01C-054: 01C-040 + 1000°C/96h/AC
01C-055: 01C-040 + 1000°C/192h/AC

01B-072: 01B-052 + 800°C/96h
01B-074: 01B-054 + 800°C/96h

01C-072: 01C-052 + 800°C/96h
01C-074: 01C-054 + 800°C/96h

01B-090: 1340°C/1.5h/FC/1210°C/AC + 800°C/48h/AC
01B-091: 1340°C/1.5h/FC/1210°C/AC + 800°C/192h/AC
01B-092: 1340°C/1.5h/FC/1300°C/AC + 800°C/47h/AC
01B-093: 1340°C/1.5h/FC/1300°C/AC + 800°C/190h/AC

An aging treatment (900°C/48h) was given to the three alloys materials that were annealed at various temperatures, followed by FC to 1200°C, and than AC to RT. The resulting Rockwell C hardness values are plotted against annealing temperature in Fig. 3.9, where the corresponding YS obtained using the relation C in Fig. 2.4. When compared with those of as-annealed materials (Fig. 2.7), the aging reduced the strength levels for all alloys. The least reduction happened for alloy 01A material, for example, with a loss of about 110 MPa (from 505 to394) for the 1360 annealing case. The most loss is observed in alloy 01C, for example, with a reduction of about 130 MPa (from 705 to 573). Apparently, all of these three alloys show an age-softening phenomenon, and the reason for this has to be investigated. Nevertheless, the remaining YS levels for alloy 01B and 01C are reasonably high with 505 MPa and 573, respectively. Changes in the lamellar microstructures, produced by the annealing at 1360°C, upon the aging (01B-013, and 01C-013) are shown in Figs. 3.10 and 3.11. It appears that the 01B lamellar material shows more changes than the 01C, Fig. 3.10. This is more obvious at a higher magnification, Fig. 3.11, where breaking up of alpha-2 plates is advanced far more for 01B material than for 01C material. Qualitatively, the lamellar spacing is coarser for both alloy materials than for K5A material. Another clear feature s the amounts of apla-2 are far less than that in K5A material. These may explain the lower YS levels for these alloys than K5A, and also the age-softening. Another important observation is that recrystallized gamma grains along the lamellar grain boundaries are much less in number and extent than for K5A. It will be very important to evaluate all these factors by testing properties including creep resistance.

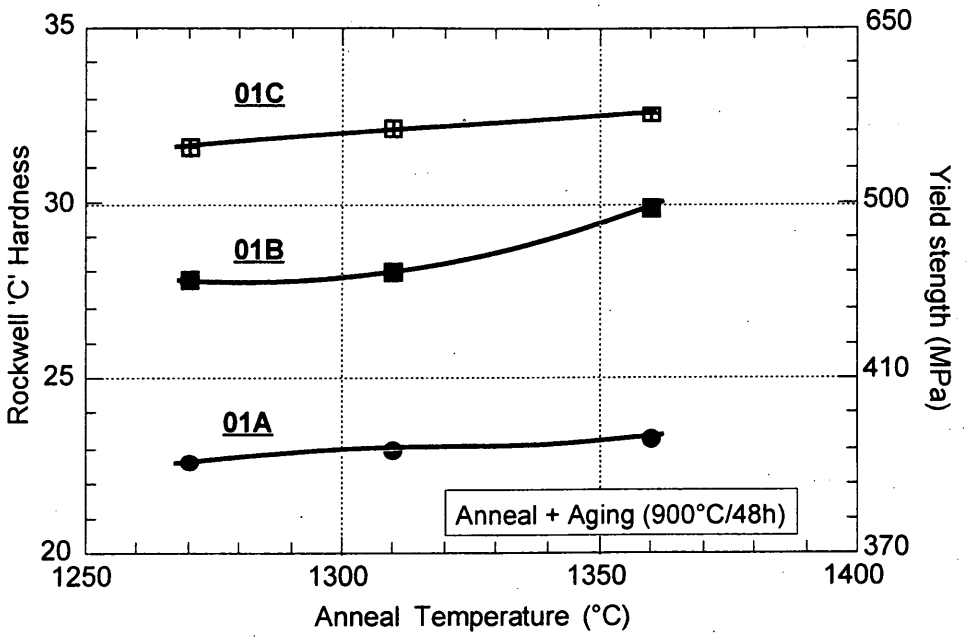

Fig. 3.9. Effect of heat treatment and aging on the Rockwell 'C' hardness values and the corresponding yield strength variations in alloys 01A, 01B and 01C. The heat treatment consisted of annealing for 2-4 hrs, followed by cooling to 1200°C at a furnace cooling rate (~60°C/min) and then air cooling to RT. A subsequent aging treatment was conducted at 900°C for 48h, followed by air cooling.

In order to understand the alpha-2 breakup process that leads to the formation of carbides and also silicides, additional aging treatments at 900°C and 1000°C on a fixed fully-lamellar condition (anneal at 1370°C) for each alloy were conducted as described below.

Alloy 01B	Alloy 01C	Anneal + Aging
01B-040	01C-040	Anneal (1370°C/2h/FC/1200°C/AC) (FL)
01B-041	01C-041	Anneal + 900°C/5h/AC
01B-042	01C-042	Anneal + 900°C/24h/AC
01B-043	01C-043	Anneal + 900°C/48h/AC
01B-044	01C-044	Anneal + 900°C/96h/AC
01B-045	01C-045	Anneal + 900°C/192h/AC
01B-051	01C-051	Anneal + 1000°C/5h/AC
01B-052	01C-052	Anneal + 1000°C/24h/AC
01B-053	01C-053	Anneal + 1000°C/48h/AC
01B-054	01C-054	Anneal + 1000°C/96h/AC
01B-055	01C-055	Anneal + 1000°C/192h/AC
01B-072	01C-072	Anneal + 1000°C/24h/AC + 800°C/96h/AC
01B-074	01C-074	Anneal + 1000°C/24h/AC + 800°C/96h/AC

Rockwell hardness measurements were made after the treatments listed above, the values were plotted as a function of aging time in Fig. 3.12. As shown, 01B-040 and 01C-040 samples had 610 and 640 MPa yield strengths, respectively, and their YS's decreased upon aging rather rapidly to reach respective plateau values which are characteristic to alloy and aging temperature. Clearly, alloy C has greater strength levels than alloy B in all conditions.

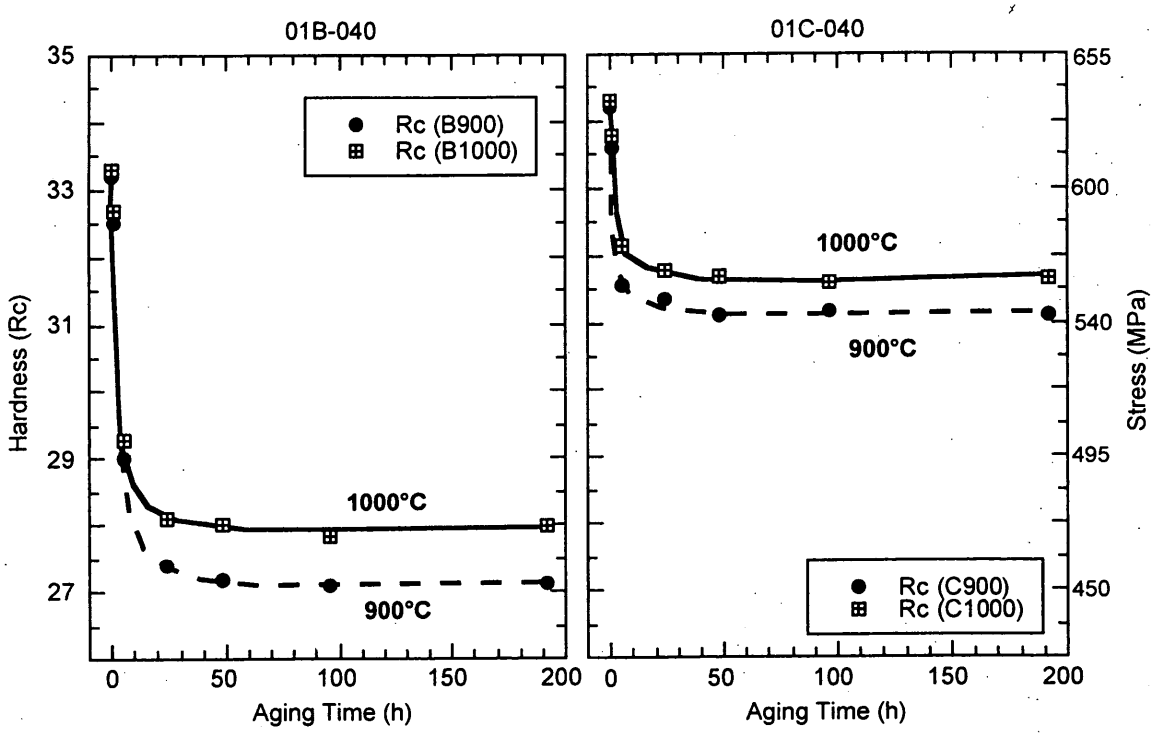

Fig. 3.12: Rockwell C (Rc) hardness variations against aging time at 900°C as well as 1000°C for both 01B-040 and 01C-040 alloy samples. Corresponding yield strength (YS) values were estimated from the Rc vs. YS relations reported in the 2nd quarter report.

The starting materials (01B-040 and 01C-040) had similar fine-grained (60-180 μm) fully-lamellar microstructures with relatively perfect lamellar arrangements as exemplified for 01B-040 in Fig. 3.13. During aging, lamellar structures became unstable, with alpha-2 plates being dissolved to reduce their volume fraction to the equilibrium. This process ended up with alpha-2 plates broken up into particles as exemplified in Fig.3.14. The broken-up alpha-2 particles are present generally in array forms along the gamma-gamma plate boundaries, although some arrays are seen to be present within gamma plates. Breakup of alpha-2 laths and the formation of carbides/silicides upon aging were observed using the high magnification BEI technique for most of cases and by TEM for some selected conditions. The latter arrangements increase the lamellar spacing or thickness, which is expected to decrease the material strength. However,

this loss may be compensated by the strengthening effects of carbides (and also silicides in case of alloy C) that are formed from the dissolving alpha-2 supersaturated with carbon. Fig. 3.15 shows BEI's of lamellar structures in two different grains of 01C-054 that was aged at 1000°C for 96h. In the grain with perfect and fine lamellar structures Fig. 3.15a, the broken up particles are present as fine stringer forms in gamma-gamma boundaries. In some cases, alpha-2 plates completely dissolve to show perfect gamma/gamma boundaries. Often, the alpha-2 plates remain unbroken although they might have undergone a thinning process with microscopic compositional segregation. In grains containing coarse, imperfect (curved) lath structures of thick gamma plates and thick, or bundles of, alpha-2 plates, breakup of alpha-2 is a fairly rapid process resulting in broad bands of fine particles Fig. 15b. Fig.3.16 shows TEM micrograpahs of 01C-054 showing arrays of gamma and broken-up alpha-2 particles bands (a) and detailed morphologies of the particles that are reasonably assumed to consist of alpha-2 particles, carbides, and silicides (b).

3.3 Process of Carbide Formation

The formation of carbides takes place from alpha-2 plates upon aging, and this can be understood by the fact that the solubilities of carbon in alpha and alpha-2 phases, $C^*(\gamma)$ and $C^*(\alpha/\alpha 2)$, are far greater than that in gamma, $C^*(\gamma)$, at any temperatures. For this, a quasi-phase diagram for the constituent phases against carbon content can be constructed as shown in Fig. 3. 17. When a sample of an alloy containing a carbon amount (Co) is cooled after an alpha annealing, the carbon concentration, $Cac(\gamma\text{-pl})$, in alpha (and later alpha-2) plates increases with decreasing temperature, while the carbon concentration, $Cac(\gamma\text{-pl})$, in the growing gamma plates is reduced as temperature decreases. When this fully-lamellar material is heat treated (including aging) below the alpha transus ($T\alpha$), the carbon concentration in the alpha-phase increases because of decreased alpha or alpha-2, volume-fractions. This pahse diagram shows the relations between the volume fraction and aging temperature and the resulting variations of in carbon concentration in alpha or alpha-2, Cage ($\alpha/\alpha 2$). Depending on the amount of Co, the increased carbon concentration can exceed the C^* (γ) (see the hatched area), resulting in the formation of carbides.

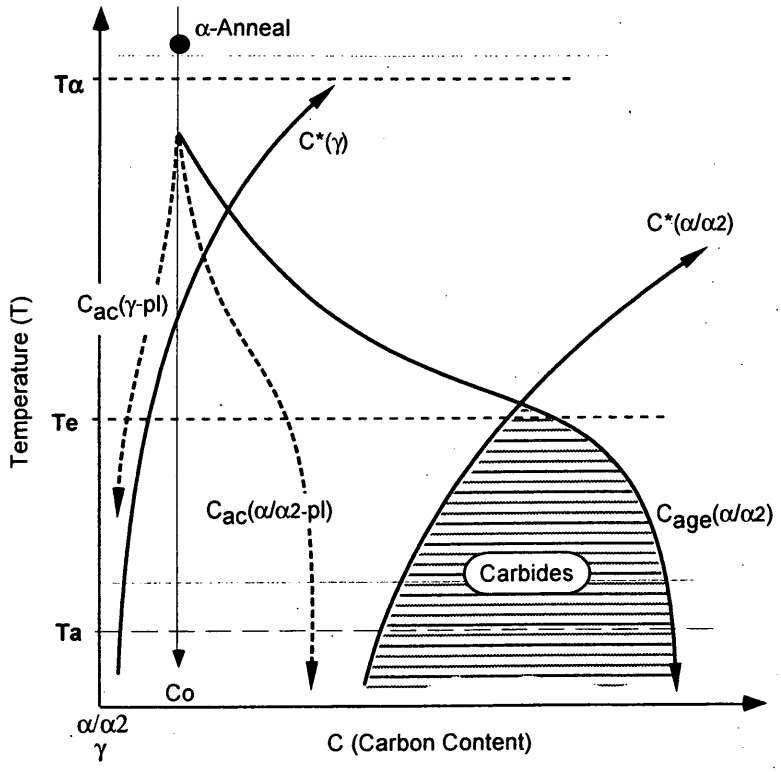

Fig. 3.17: Pseudo phase diagram for α/α2-carbon and γ-C in a phase gamma alloy having a carbon content (Co), relating the carbon solubilities (C*) in the constituent phases and the carbon concentrations in the lamellar structure in an as-cooled condition (Cac) and after aging (Cage).

The presence of carbide particles and alpha-2 breakups may effectively alter the perfect gamma/gamma boundary nature and effects. According to the phase relations in Fig. 3. 17, a two-step aging process can be designed such that carbides are distributed in band forms, instead of stringer forms. Trials were made on alloys 01B and 01C by employing a two-step aging treatment. One example was 01C-072 (1370°C/2h/FC/1200°C/AC + 1000°C/24h/AC + 800°C/96h). The resulting distribution of various particles in a grain containing coarse lamellar structures is shown in Fig. 3.18. The high temperature (1000°C) aging results in the formation of carbides as well as gamma phase bands highly concentrated with C and silicides, around the remaining alpha-2. Upon the low temperature aging, additional, finer carbide particles form from the gamma region by the segregation of excess amounts of carbon due to the lower solubility of carbo

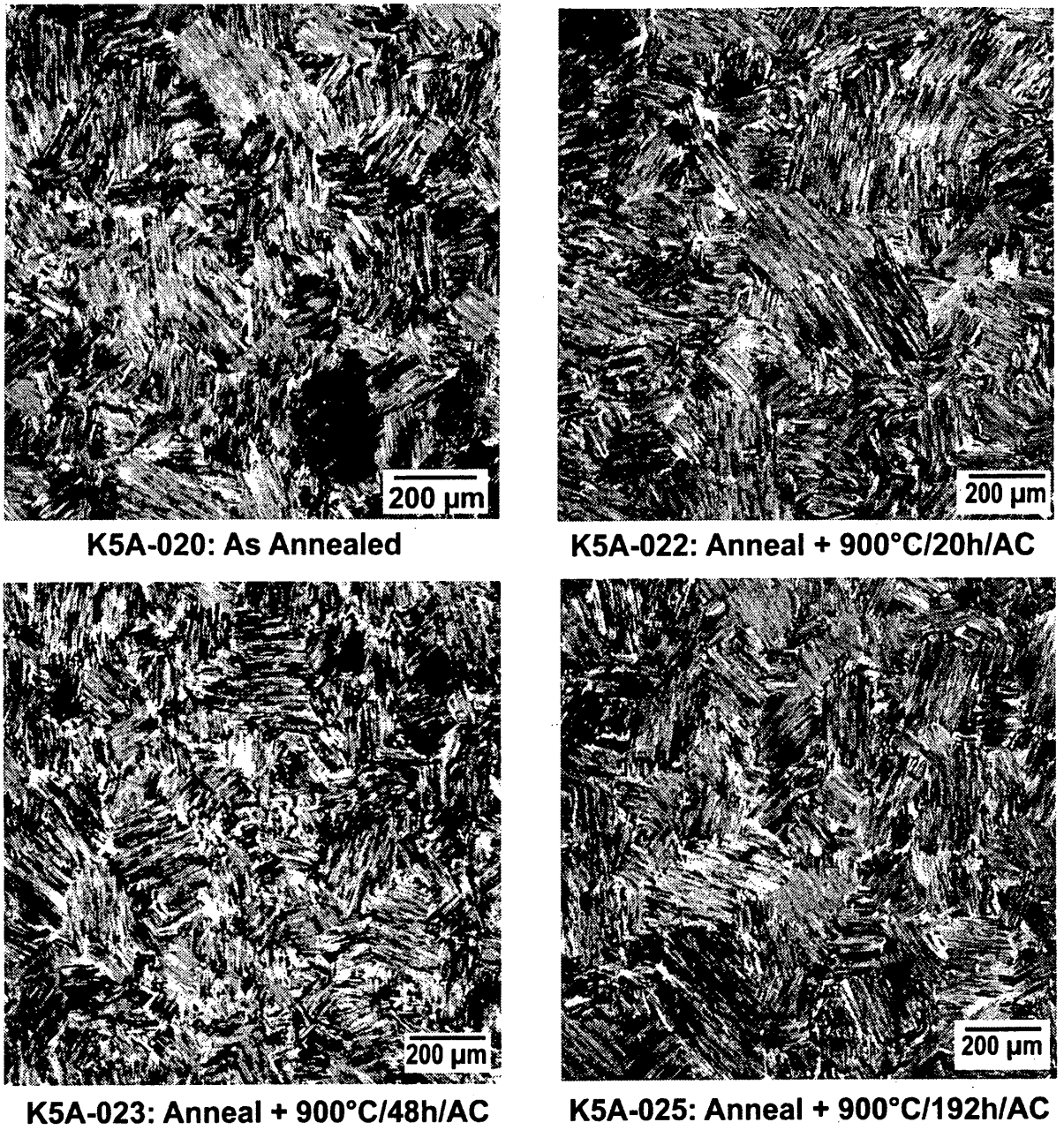

Fig. 3.2: Effect of isothermal aging at 900°C on the fully-lamellar (FL) microstructure developed in K5A forged material that was annealed at 1320°C for 1h and then cooled to 1100°C at a cooling rate of 50°C/min, immediately followed by air cooling to RT.

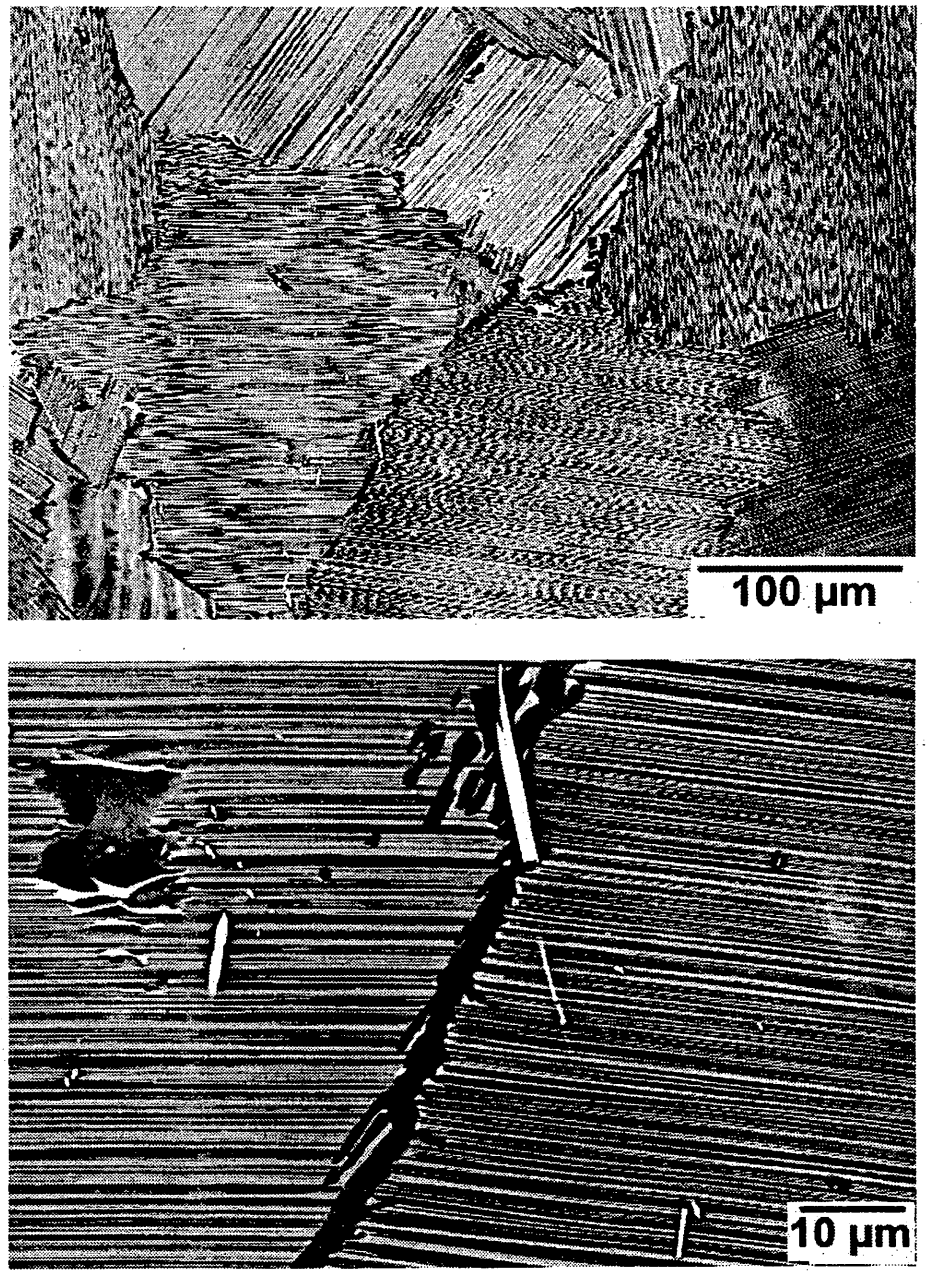

Fig. 3.3: Back-scattered electron (BSE) image of the as-annealed FL microstructure (K5A-020) in Micrograph 3. This FL microstructure consists of relatively fine grains having an average size of about 150 µm, and fine lamellar spacing. While most of grain boundaries are ragged, the continuous gamma phase occasionally constitutes the boundaries.

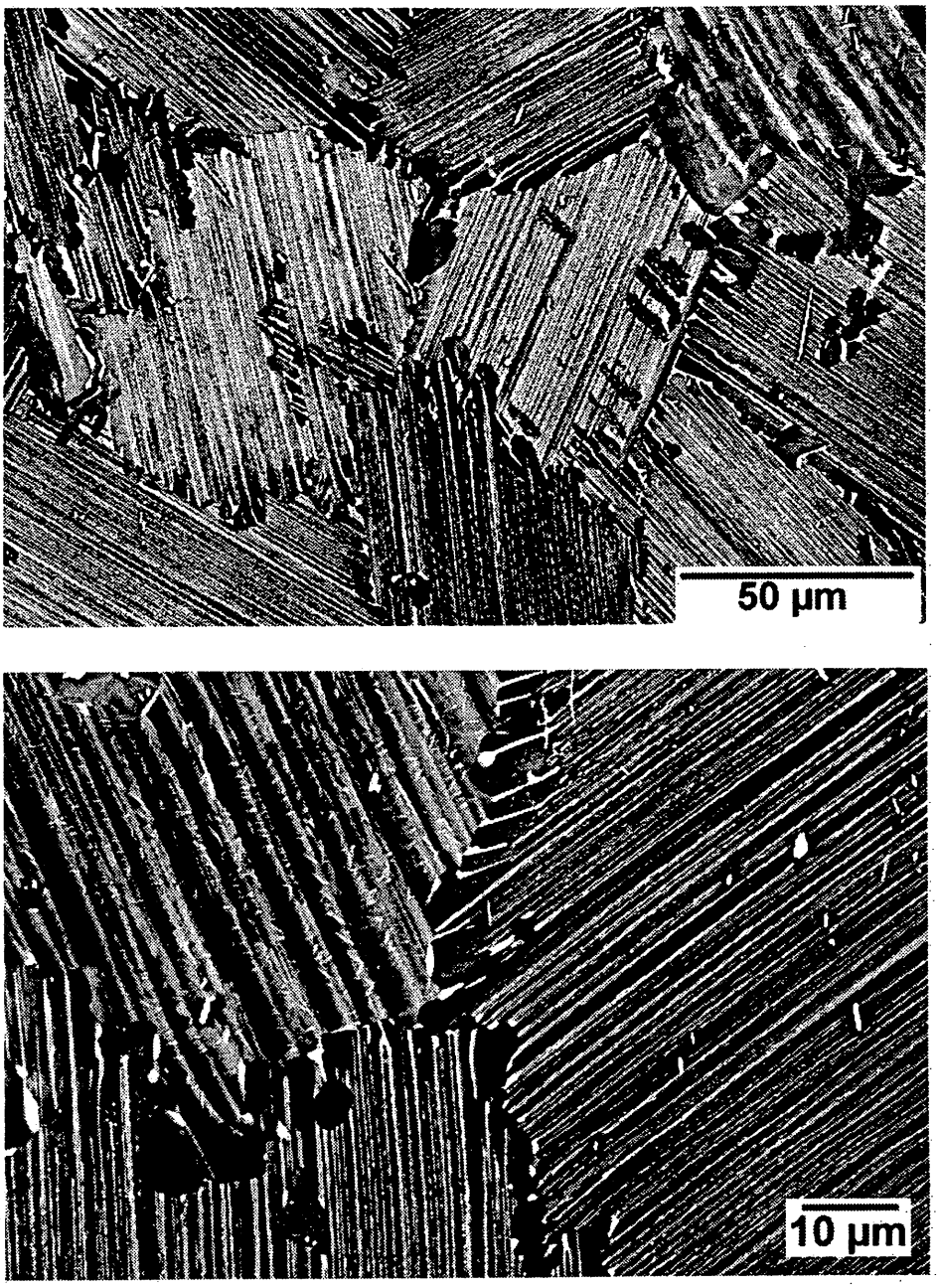

K5A-023: 1320°C/1h/50°C/min/1100°C/AC + 900°C/48h/AC

Fig. 3.4: Back-scattered electron (BSE) image of the FL microstructure after aging at 900°C for 48h (K5A-023). Alpha-2 plates (imaged bright) begin to be broken up into various shapes, and gamma grains (imaged dark/gray) are generated at or near grain boundaries as the result of recrystallization.

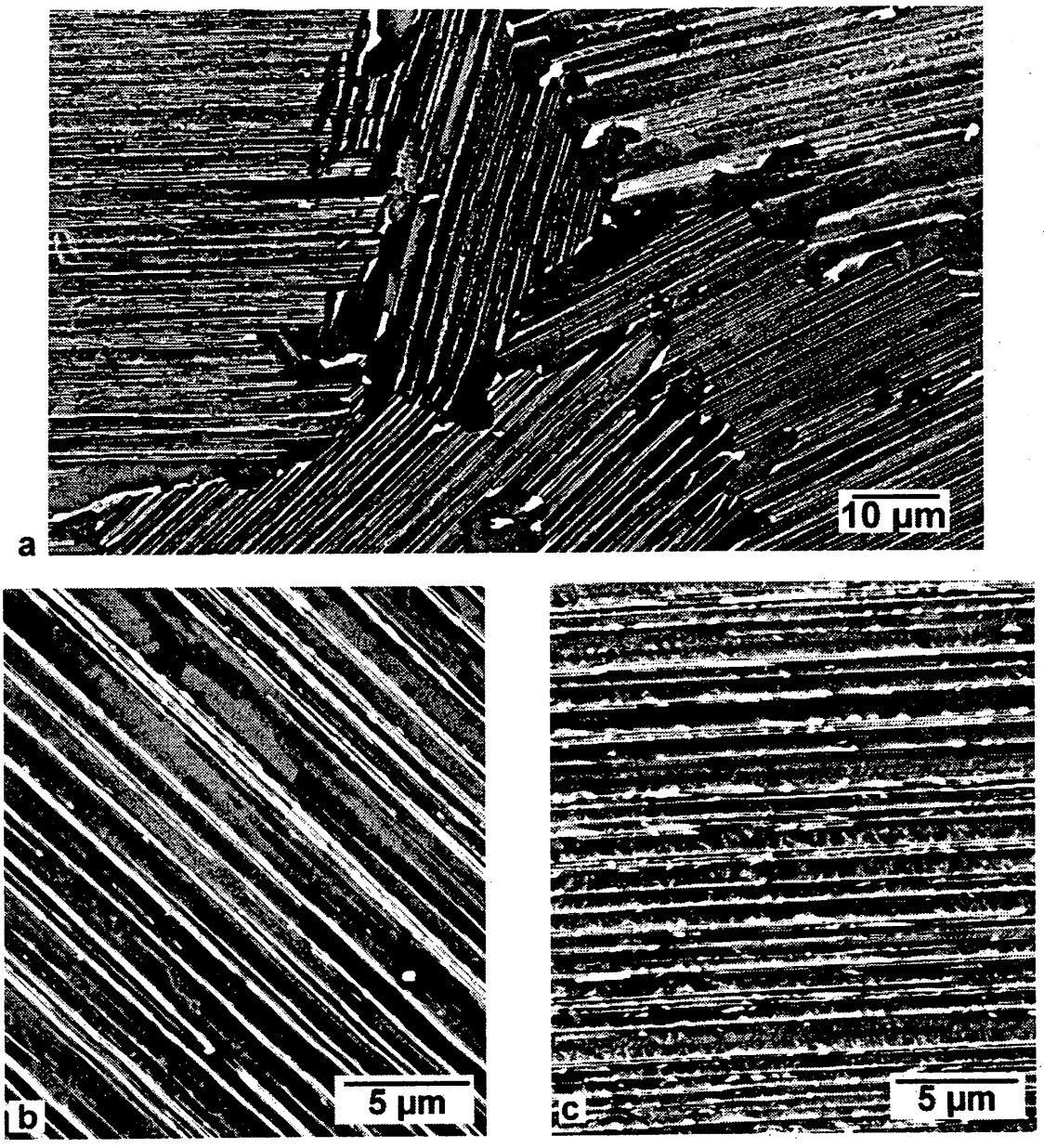

Fig. 3.5: Back-scattered electron (BSE) image of the FL microstructure after aging at 900°C for 96h (K5A-024). Breakup of alpha-2 plates (imaged bright) has extended, while in some grains they are still continuous. Gamma grains (imaged dark/gray) along grain boundaries appear more abundant indicating further progress of recrystallization.

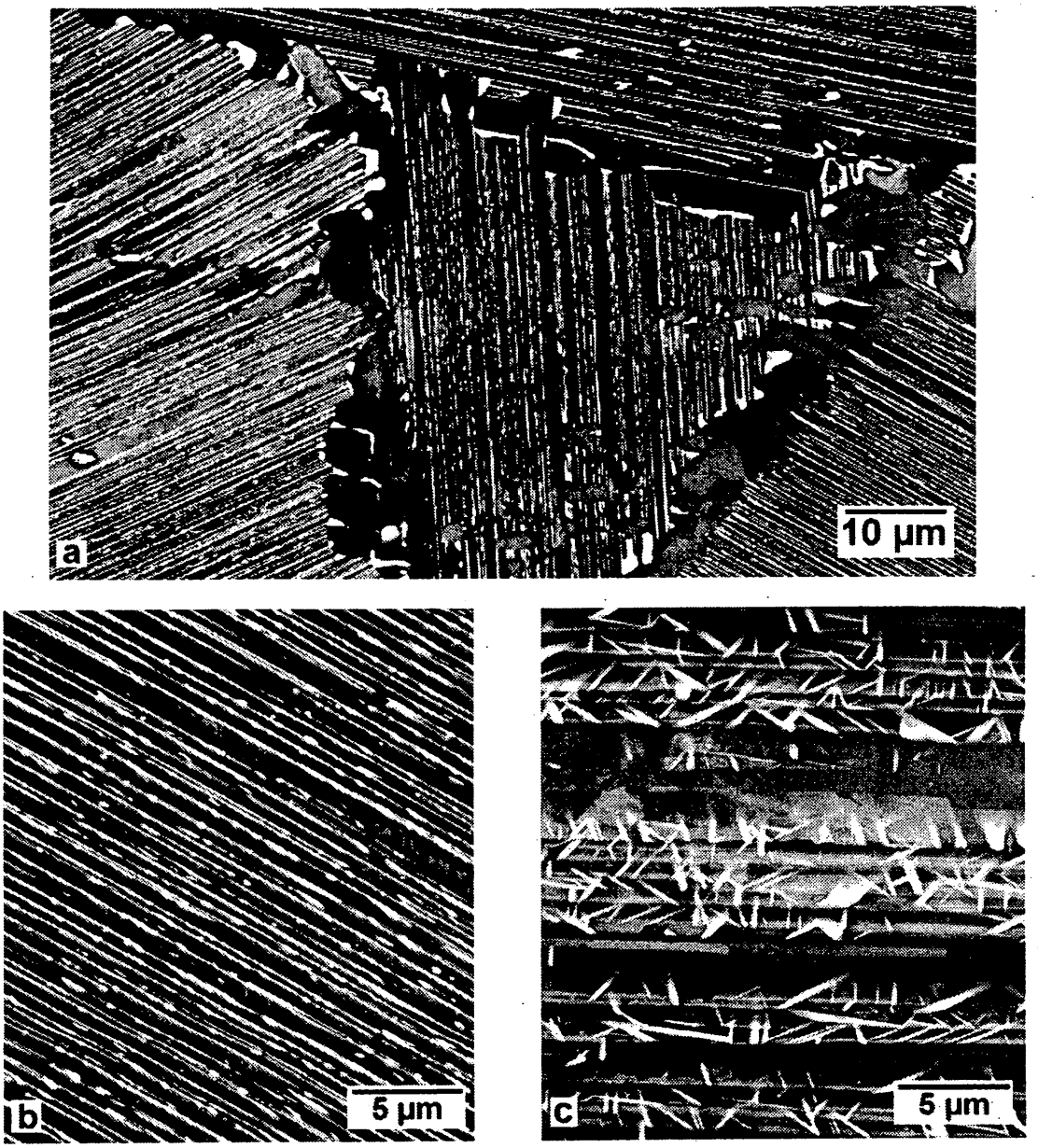

Fig. 3.6: Back-scattered electron (BSE) image of the FL microstructure after aging at 900°C for 192h (K5A-025). Breakup of alpha-2 plates (imaged bright) is extensive, although in some grains some segments are still continuous. Gamma grains (imaged dark/gray) along grain boundaries appear almost entirely interconnected to separate lamellar grains from the neighboring ones

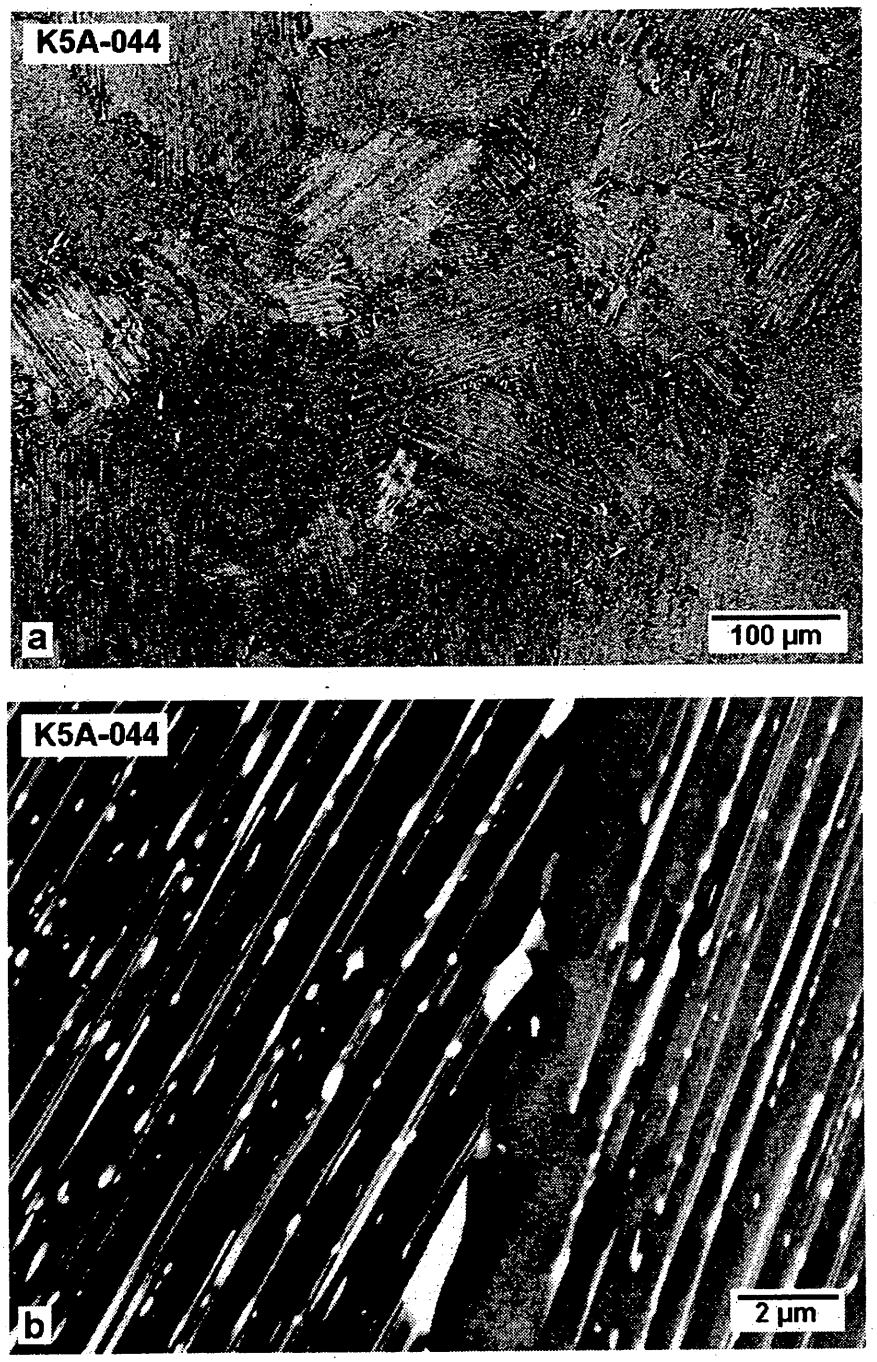

Fig. 3.8A: SEM-BEI of microstructures of K5A-044 (alpha anneal + 900°C/336h), showing fully-lamella microstructures at a low magnification (a) and stringers of alpha-2 plates and particles, beta particles (imaged brightest), and carbides at a high magnification

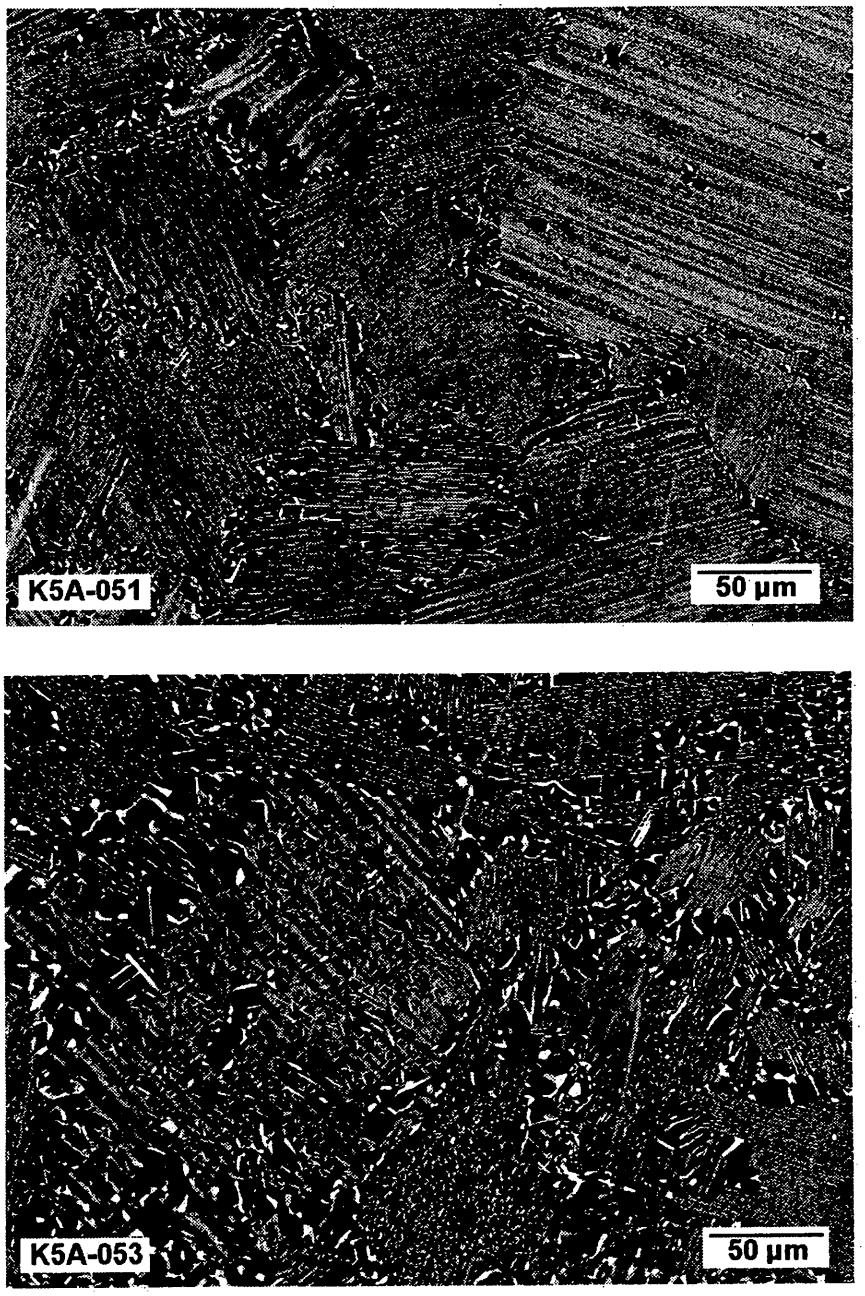

Fig. 3.8B: SEM-BEI of fully-lamellar microstructures of K5A-031 after aging at 1000°C/24h (K5A-51) and 1000°C/168h (K5A-033). Excessive growth of gamma grains (imaged dark) is seen in the K5A-053 condition.

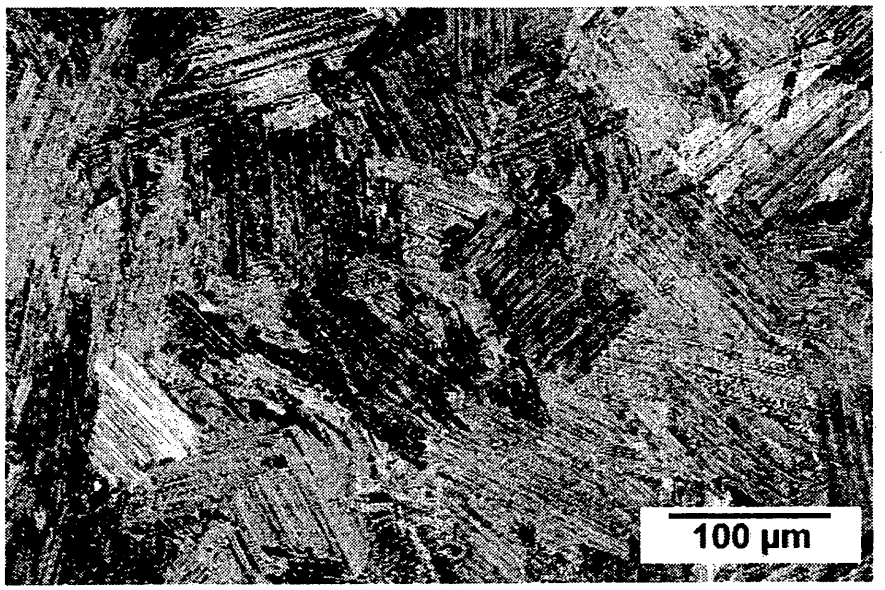

01B-013: 1360°C/2h/FC/1200°C/AC + 900°C/48h/AC

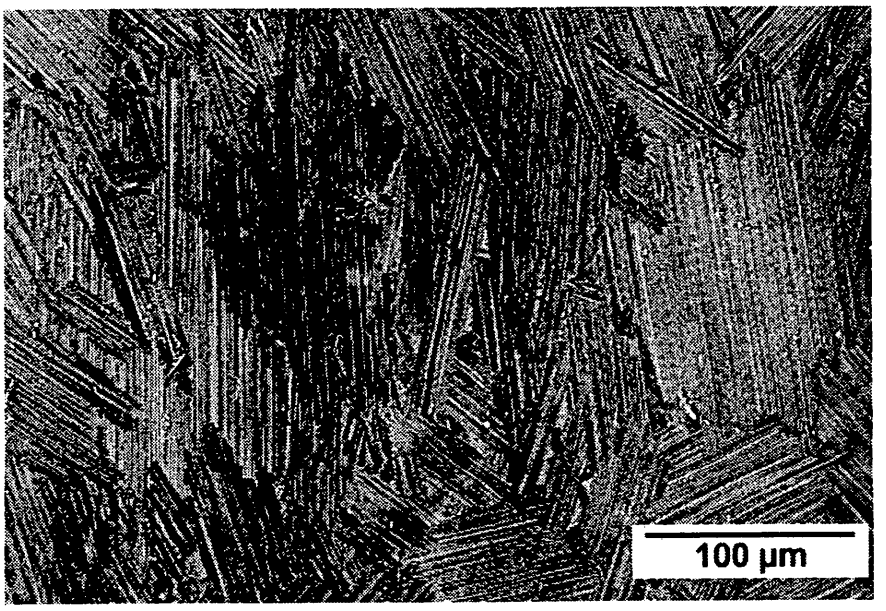

01C-013: 1360°C/2h/FC/1200°C/AC + 900°C/48h/AC

Fig. 3.10: Back-scattered electron images showing the effect of an aging (900°C/48h) on the FL microstructure produced by annealing at 1360°C for 2h and then furnace cooling (60°C/min) to 1200°C followed by air-cooling to RT (01X-005). The aging appears to have disturbed lamellar structures somewhat, especially, for 01B alloy.

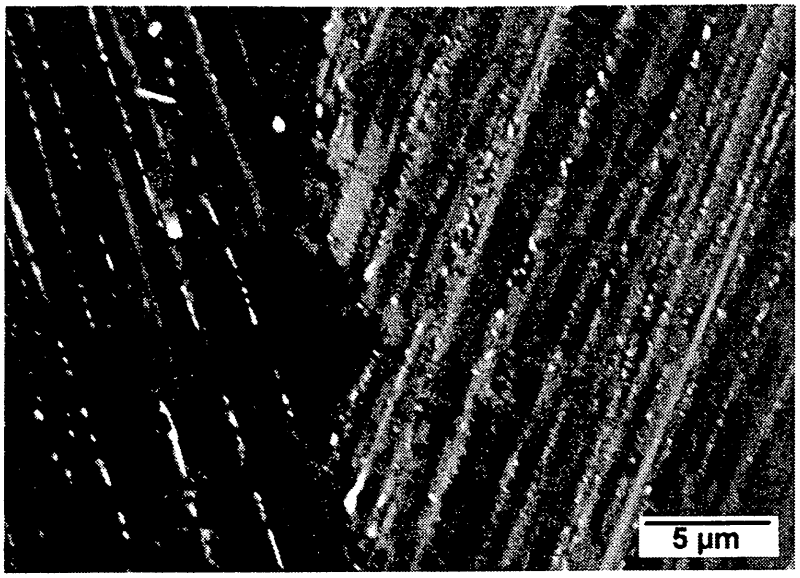

01B-013. 1360°C/2h/FC/1200°C /AC+900°C/48h/AC

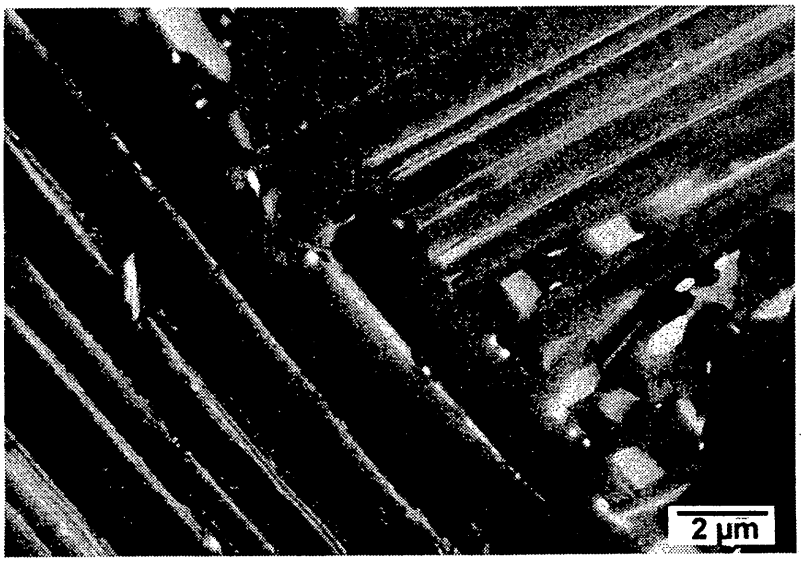

01C-013 1360°C/2h/FC/1200°C/AC+900°C/48h/AC

Fig. 3.11: Back-scattered electron images of 01B-013 and 01C-013 (see Fig. 3.10) at higher magnifications showing the lamellar structures and the alpha-2 phase distribution. The aging resulted in breaking up the alpha-2 plates into fine particles in alloy 01B while in 01C the breaking-up process appears to have been under way.

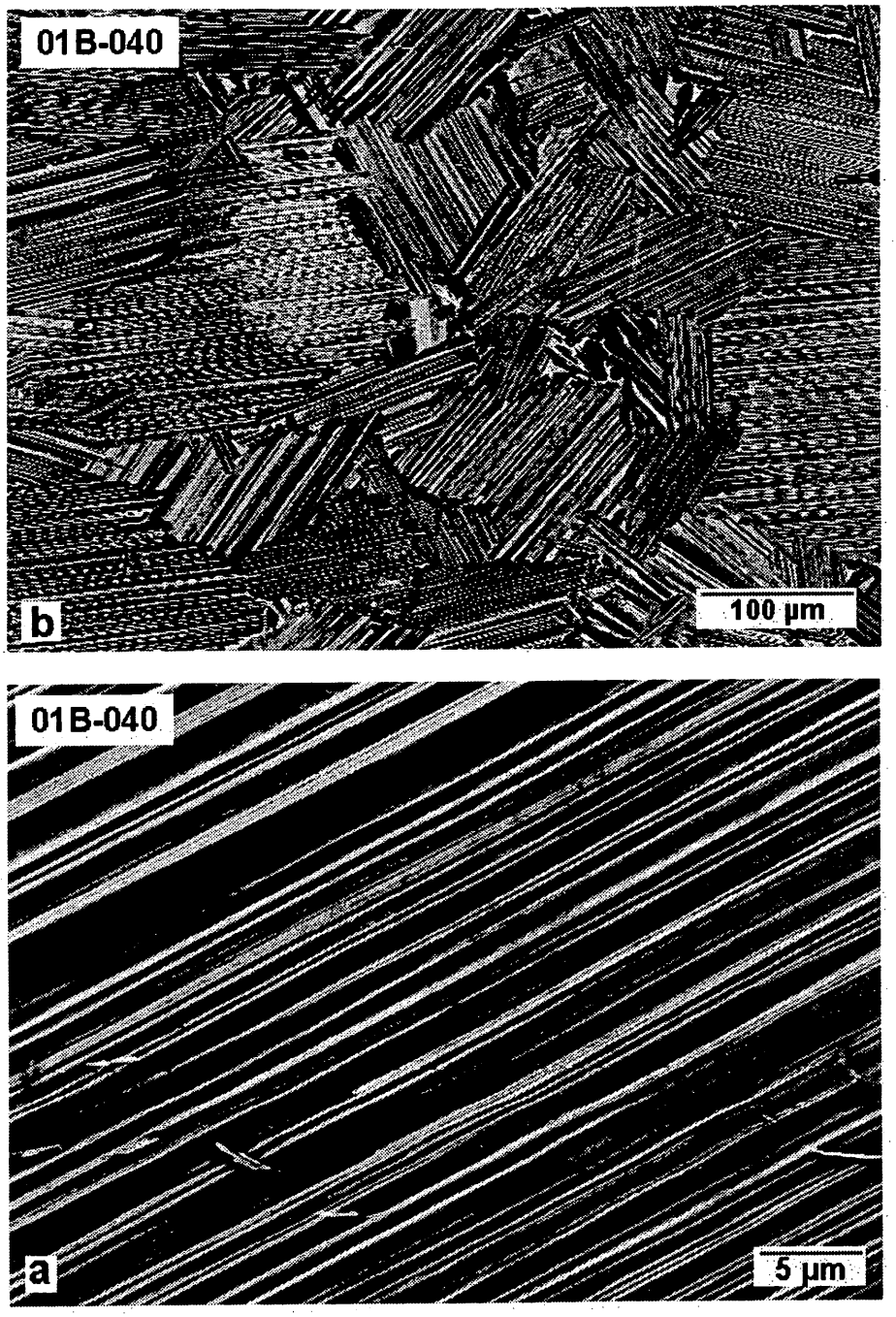

Fig. 3.13: SEM-BEI micrographs of alloy 01B-040 (1370°C/2h/FC/1200°C/AC) fully-lamellar microstructure showing grain sizes and distribution (a) and a perfect lamellar arrangement within a grain (b). Borides flakes are also shown in b.

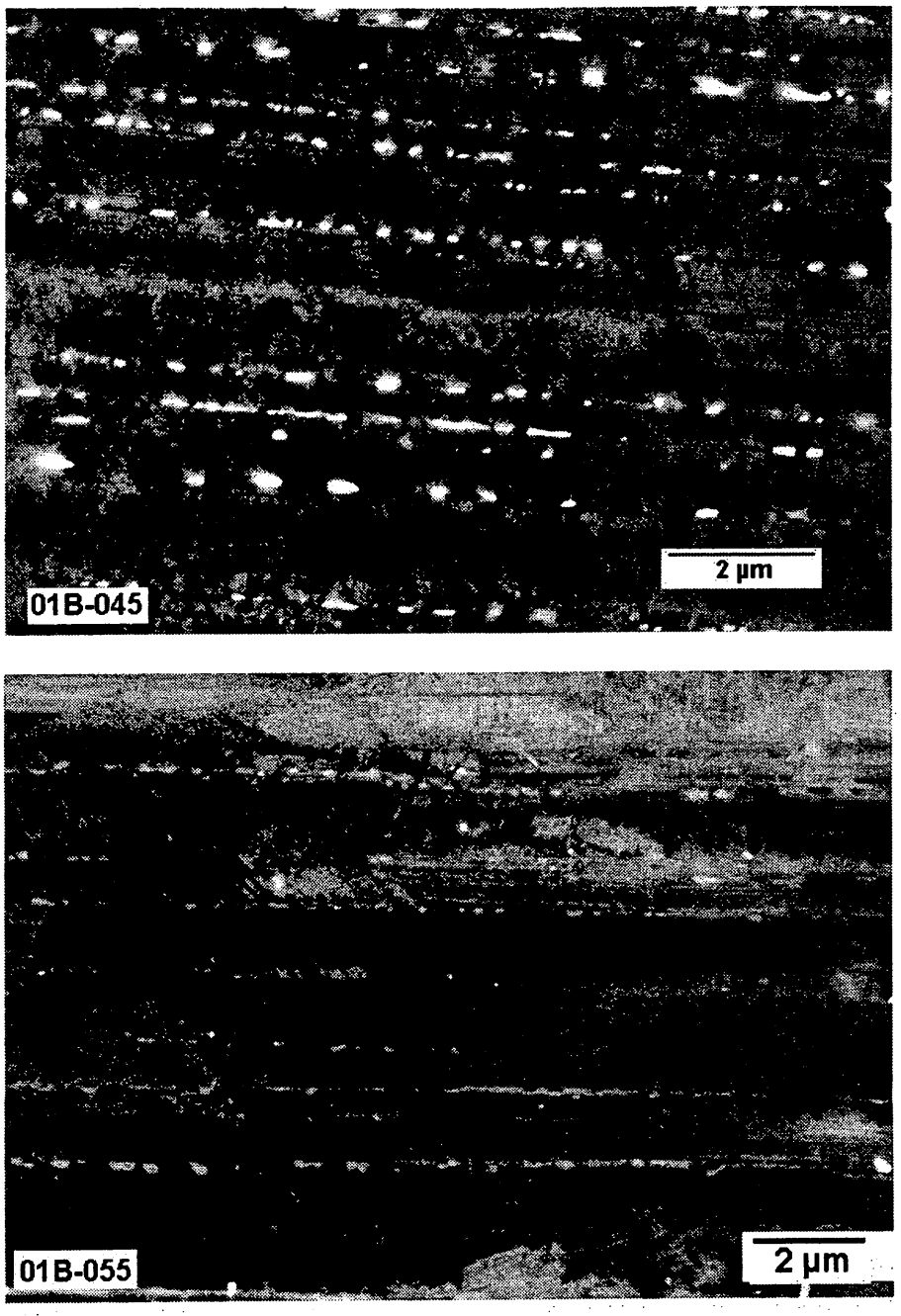

Fig. 3.14: SEM-BEI micrographs of the lamellar microstuctures of 01B-040 material after aging at for 192 h at 900°C (01B-045) and 1000°C (01B-055) showing broken-up alpha-2 particle arrays. It appears that alpha-2 volume particles are reduced in size as well as volume with increasing aging temperature.

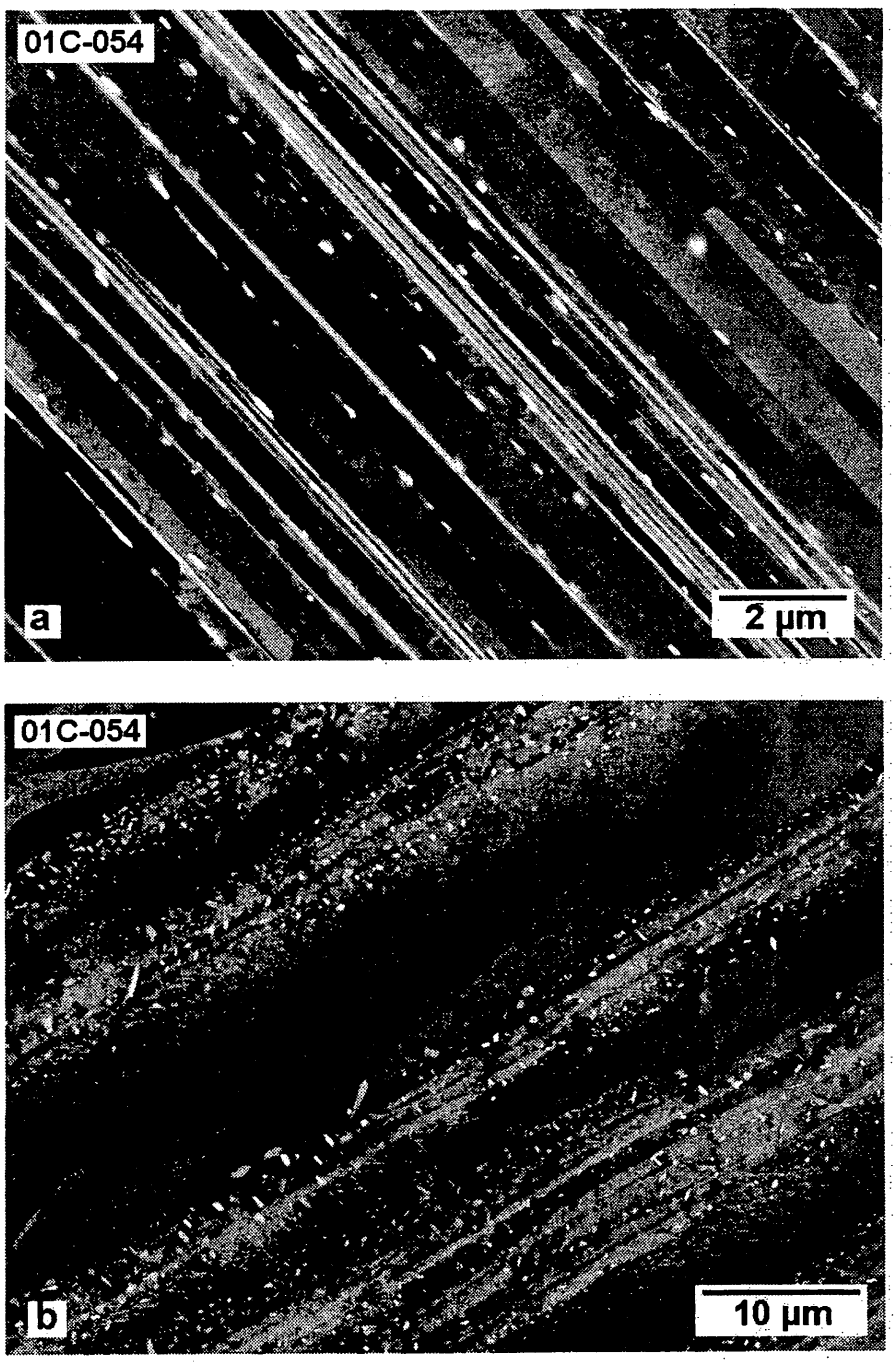

Fig. 3.15: SEM-BEI micrographs of lamellar microstructures in two different grains of 01C-054 (anneal + 900°C/96h/AC) showing different types of alpha-2 break-up and their distribution. Break-up is a slow process in perfect lamellar structures (a) while the process is relatively rapid to produce both alpha-2 and carbide/silicide distribution more randomly for coarse and irregular lamellar structures (b)

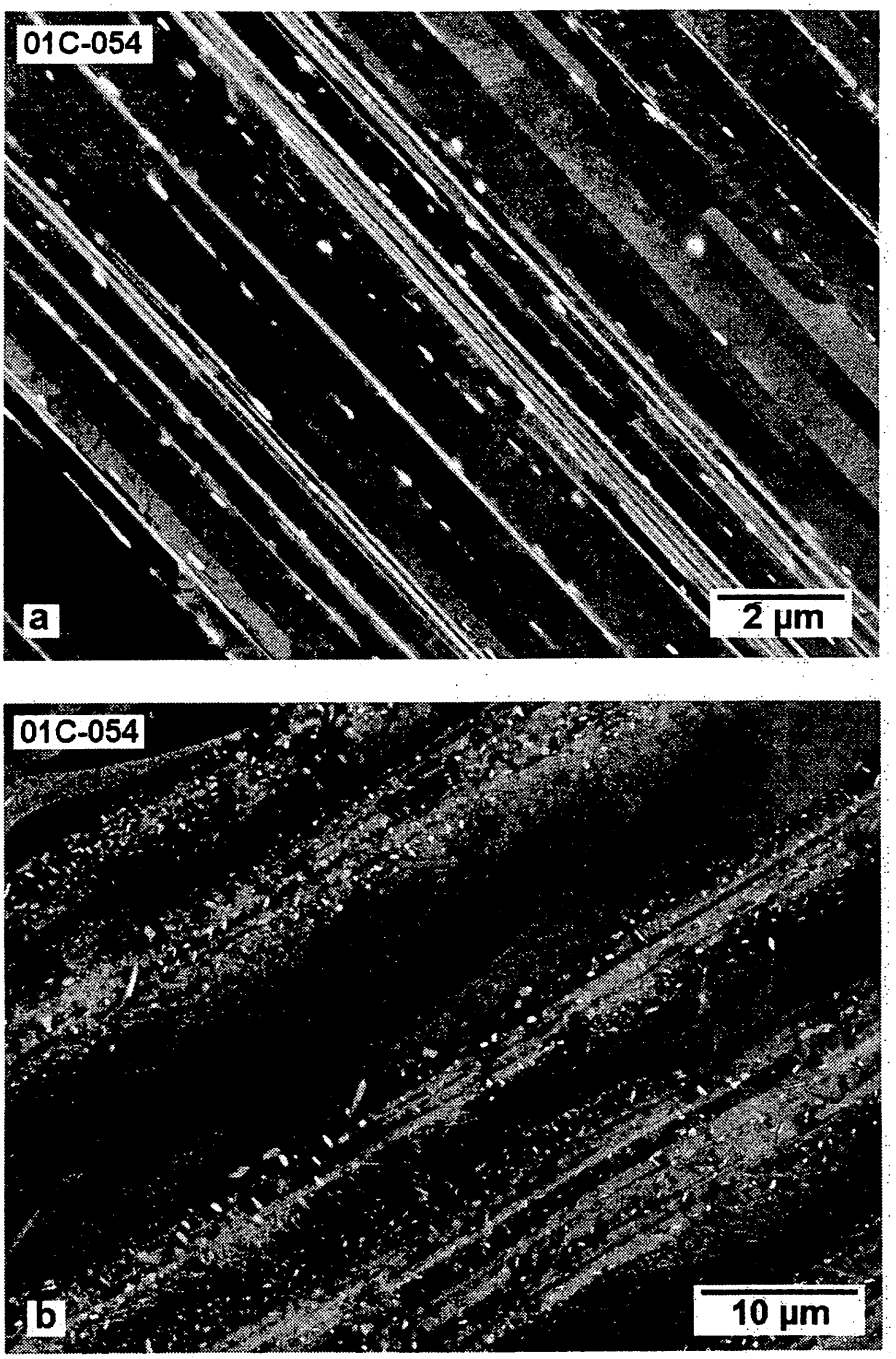

Fig. 3.15: SEM-BEI micrographs of lamellar microstructures in two different grains of 01C-054 (anneal + 900°C/96h/AC) showing different types of alpha-2 break-up and their distribution. Break-up is a slow process in perfect lamellar structures (a) while the process is relatively rapid to produce both alpha-2 and carbide/silicide distribution more randomly for coarse and irregular lamellar structures (b)

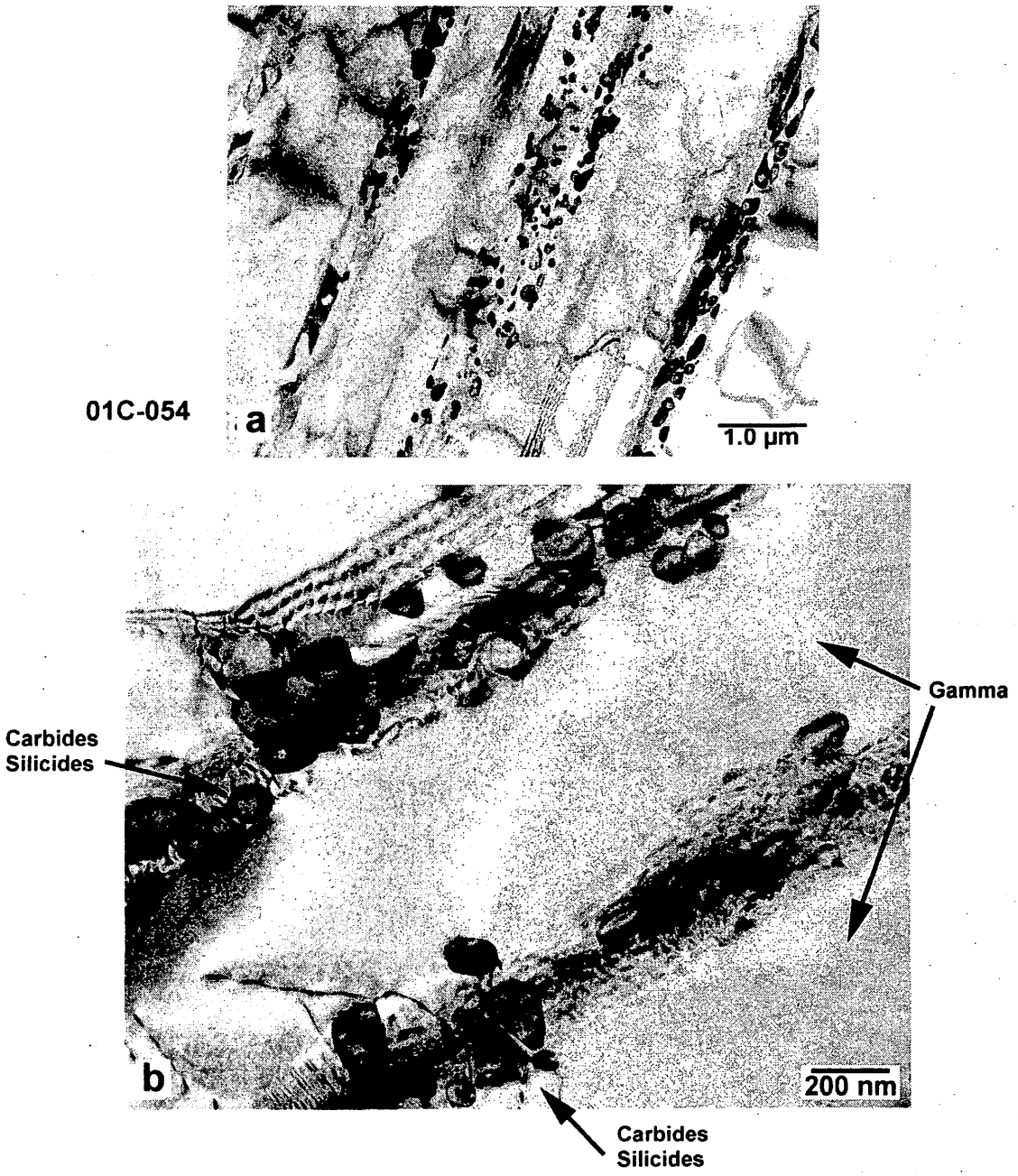

Fig. 3.16: TEM micrographs of microstuctures of 01C-054 (1000°C/96h) showing arrays of gamma and broken-up alpha-2 particle bands (a) and the particles in the bands (b).

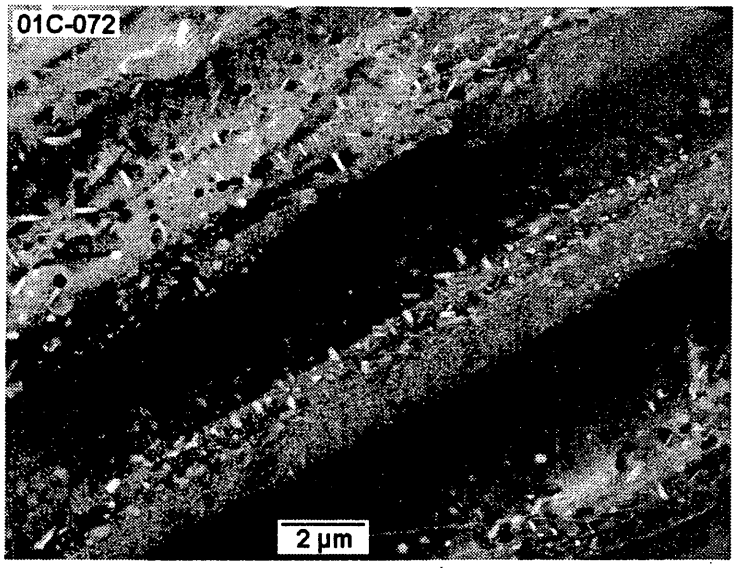

Fig. 3.18: BEI of a feature typically observed in the lamellar microstructures in 01C-072 condition (1370°C/2h/FC/1200°C/AC + 1000°C/24h/AC + 800°C/96h) showing fine carbide particles (mostly imaged dark) and silicides (rod-like, mostly imaged bright) that may have been formed during the second step aging at 800°C.

4.0 Property Evaluation

Mechanical property evaluation was conducted on FL materials in selected aging conditions described in Table 4.1.

Table. 4.1: Heat Treatment (Anneal + Aging) Conditions of Creep Test Specimens

01A-031:	1000°C/3h/FC/RT + 1360°C/2h/FC/1200°C/AC + 900°C/48h/AC
01B-031:	1000°C/3h/FC/RT + 1360°C/2h/FC/1200°C/AC + 900°C/48h/AC
01C-031:	1000°C/3h/FC/RT + 1360°C/2h/FC/1200°C/AC + 900°C/48h/AC
01B-032:	1000°C/3h/FC/RT + 1370°C/2h/FC/1200°C/AC + 900°C/48hAC
01C-032:	1000°C/3h/FC/RT + 1370°C/2h/FC/1200°C/AC + 900°C/48h/AC
01C-081:	1360°C/2h/FC/1200°C/AC + 900°C/72h/AC + 800°C/120h/AC
01C-082:	1360°C/2h/FC/1200°C/AC + 1000°C/27h/AC + 800°C/162h/AC
01D-081:	1330°C/2h/FC/1200°C/AC + 900°C/72h/AC + 800°C/119h/AC
01D-082:	1330°C/2h/FC/1200°C/AC + 1000°C/27h/AC + 800°C/162h/AC

Microstructures under a polarized light condition in the 031 heat treatment (annealing + aging) condition are shown in Fig. 4.1. As shown, a nearly lamellar (NL) microstructure was produced in alloy 01A (Fig. 4.1a), whereas randomly oriented TMY lamellar structures were introduced in alloys 01B and 01C (Fig. 4.1b and 4.1c). Lamellar grain sizes of 01B-031 and 01C-031 are roughly the same (approximately 120 μm), while the lamellar spacing in 01C-031 clearly finer than that in 01B-031. Though not shown here, microstructures generated by the 032 HT condition (01B-032 and 01C-032) are similar to those of 01B-031 and 01C-031 condition. Figs. 4.2 show TMT lamellar microstructures in alloy 01C generated by the 081 and 082 conditions, exhibiting similar features in spite of considerably different aging conditions. This indicates that the lamellar structures are reasonably stable, as they appear at low magnifications, thermally up to 1000°C. As shown later, however, these two conditions show different creep responses, indicating the microstructures differ in finer scale. In fact, though not shown here, 082 aging resulted in coarser breakups, and FL grains are decorated with more expanded gamma grains and bands. Similar observations were made in 01D-081 and 01D-082 materials as shown in Fig. 4.3

RST + 1360°C/2h/FC/1200°C/AC + 900°C/48h/AC

01A-031

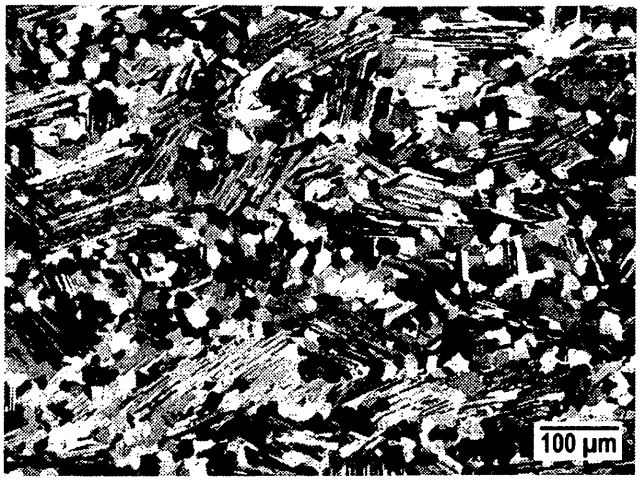

01B-031

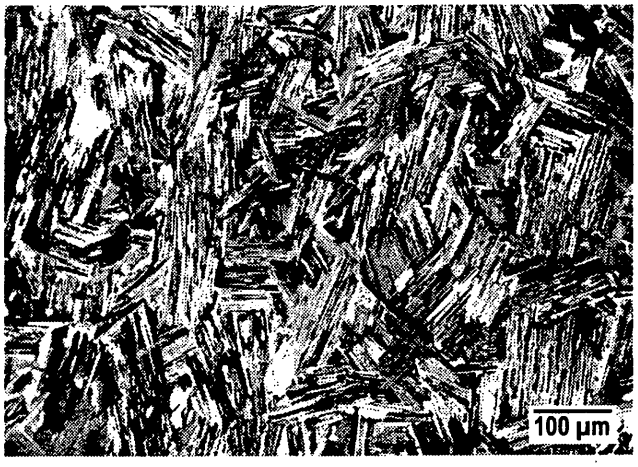

01C-031

Fig. 4.1: Polarized light microstructures of three alloys that were produced through annealing at 1350°C/2h, furnace cooling to 1200°C, followed by air cooling to RT, and then subsequent aging at 900°C for 48h (01X-031). The materials were supplied for GRC to evaluate their creep resistance.

01C-081: 01C-080 + 900°C/72h + 800°C/119h

01C-082: 01C-080 + 1000°C/27h/AC + 800°C/162h

Fig. 4.2: TMT lamellar microstructures in alloy 01C material stabilized in two different aging conditions for mechanical testing (01C-080: 1360°C/2h/FC/1200°C/AC)

K5A-082: K5A-080 + 1000°C/27h/AC + 800°C/162h

K5A-081: K5A-080 + 900°C/72h + 800°C/119h

Fig. 4.3: TMT lamellar microstructures in alloy 01D material stabilized in two different aging conditions for mechanical testing (01D-080=K5A-080: 1330°C/2h/FC/1200°C/AC)

4.1 Tensile Properties

RT tensile testing was conducted on alloys 01B, 01C and 01D in all conditions at RT at a strain rate of 0.0002/sec, and the results are listed in Table 4.2. From these, their properties were plotted for comparison in Fig. 4.4 In 032 materials condition, Alloy 01B shows better ductility, whereas alloy 01C has greater yield as well as tensile strengths. Even for alloy 01C, however, the ductility is greater than 1%. This, along with fairly fine grain sizes (~120 μm) and good strength levels, is expected to yield excellent fatigue resistance in alloy 01C. However, increasing aging temperature and time reduces strength but appears to increase ductility. As analyzed earlier, this is largely due to increases in gamma plate thickness and reduction of alpha-2 plate/volume. The distribution of carbides and silicides has not been characterized in detail. Alloy 01D (K5A) exhibits the highest strength and the lowest ductility. The lowest aluminum content in 0iD alloy will yield the highest volume fraction of alpha-2 phase (with a composition around Ti-38Al) that is known to have higher strength but lower strain-to-failure (believed to be caused by the Al content much higher than for Ti3Al) than gamma phase. There appears to be a clear trend that increases in strength result in lowering ductility.

Table 4.2: Tensile Properties of 01C and K5A in Various Anneal/Aging Conditions

Specimen	YS (MPa)	UTS (MPa)	Et (%)	Epl (%)	E (GPa)
01B-032	476	596	1.8		
01B-032	464	582	1.3		
01C-032	574	643	1.1		
01C-032	541	645	1.2		
01C-081	495	613	1.34	1.06	175
01C-081	490	624	1.53	1.25	174
01C-082	474	578	1.37	1.10	174
01C-082	481	598	1.47	1.19	169
K5A-081	654	687	0.71	0.31	155
K5A-081	648	698	0.75	0.35	154
K5A-082	660	712	0.82	0.42	162
K5A-082	661	708	0.82	0.41	153

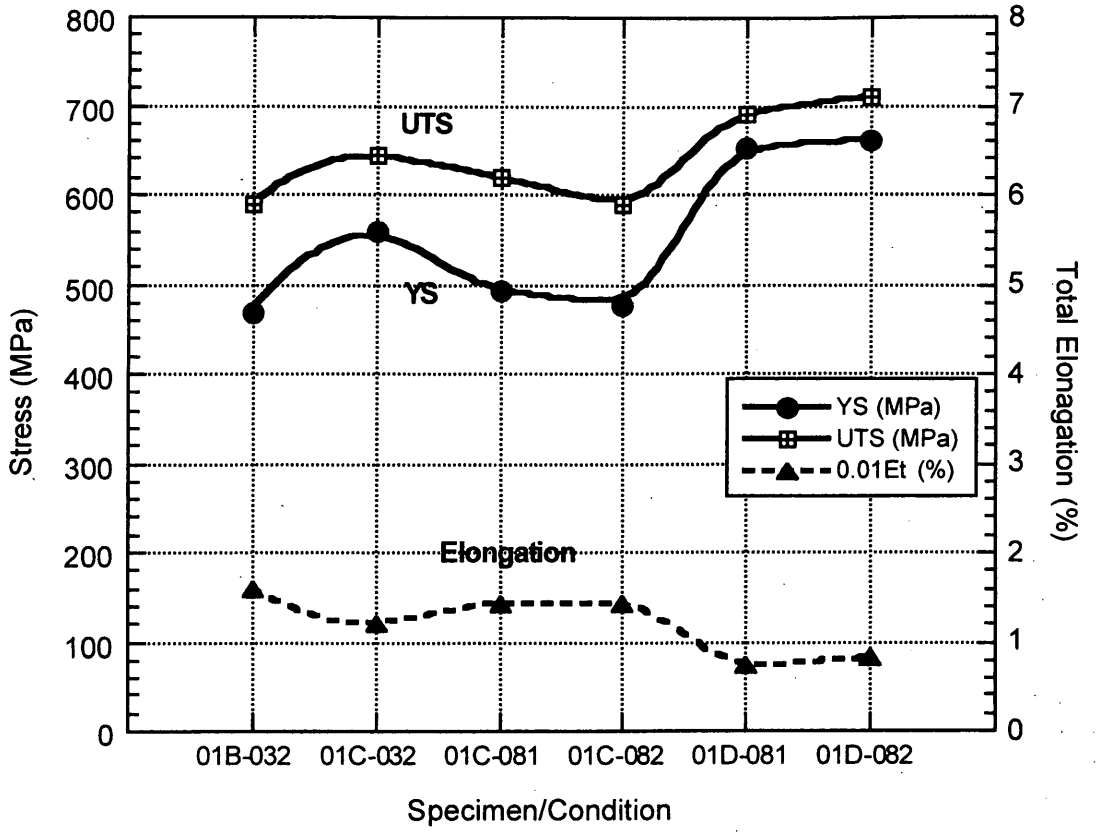

Fig. 4.4: RT Tensile Properties of 01B, 01C and 01D in Fully-Lamellar and Aged Conditions

Table 4.1 also shows another interesting feature, that is, the dependence of elastic modulus (E) on the composition. 01C alloy exhibits a greater modulus (174GPa) compared for that (lower than 160GPa) of 01D (K5A) alloy material. Clearly, lowering Al content reduces the modulus, and this can be explained by increased volume fraction of alpha-2 that will lower the modulus of the two-phase alloy system.

4.2 Creep Properties

Creep testing has been conducted at 704°C, 760°C, 815°C and 870°C in air on 01C alloy in 01C-032 and 01C-081 and 082 conditions. Two types of loading conditions were employed: the first is the stress increment method and the other is a constant load condition. The details are listed in Table 4.3. Creep curves collected under constant stress (290Mpa) loading at 704°C are plotted in Fig. 4.5. As shown, 01C-032 exhibits the least creep strain or

the best creep resistance in these conditions, for example, with the time to 1% strain being about 1000h. 01C-082 yielded greater creep resistance than 01C-081. This is unexpected because both have similar RT tensile strengths (see table 4.4) and because 01C-082 received the most extensive aging treatment (see Table 4.1). These results have yet to be further analyzed by conducting additional testing.

Table 4.3: Creep Specimens Material Conditions (01C Alloy) and Test Conditions

Spec. No	HT Condition	T (°C)	Loading Condition (MPa)
C205	01C-032	760	Step Increase: 207-276-345-414
C206	01C-032	870	Step Increase: 104-173-242
C207	01C-032	760	Step Increase: 138-173-207-242-276-311
C208	01C-032	815	Step Increase: 104-138-173-207-242
C209	01C-032	704	Constant Load: 290
C211	01C-081	704	Constant Load: 290
C214	01C-082	704	Constant Load: 290

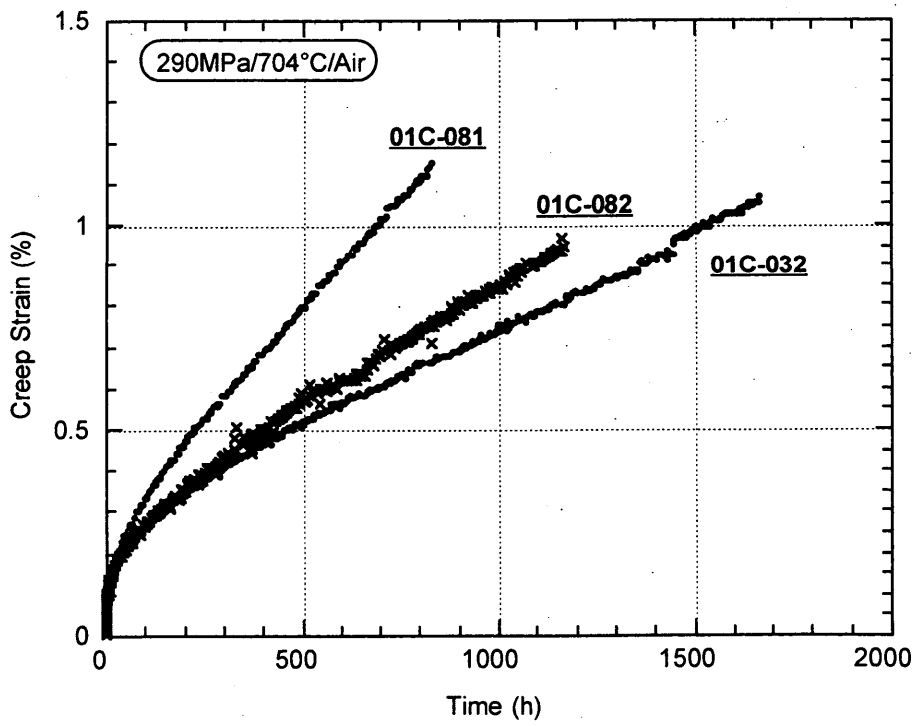

Fig. 4.5: Creep curves of alloy 01C in three different HT (Anneal + Aging) conditions (see Table 4.1) tested at 704°C in air under a constant load that corresponds to 290Mpa

Fig. 4.6 shows creep curves of 01C-032 material tested under the stress increase creep conditions at 760°C and 815°C. The curves are plotted in two different fields; that is, in linear-linear scale (Fig. 4.6a) and linear-log scale (Fig. 4.6b). The latter scale was selected to show better the initial low strain stages.

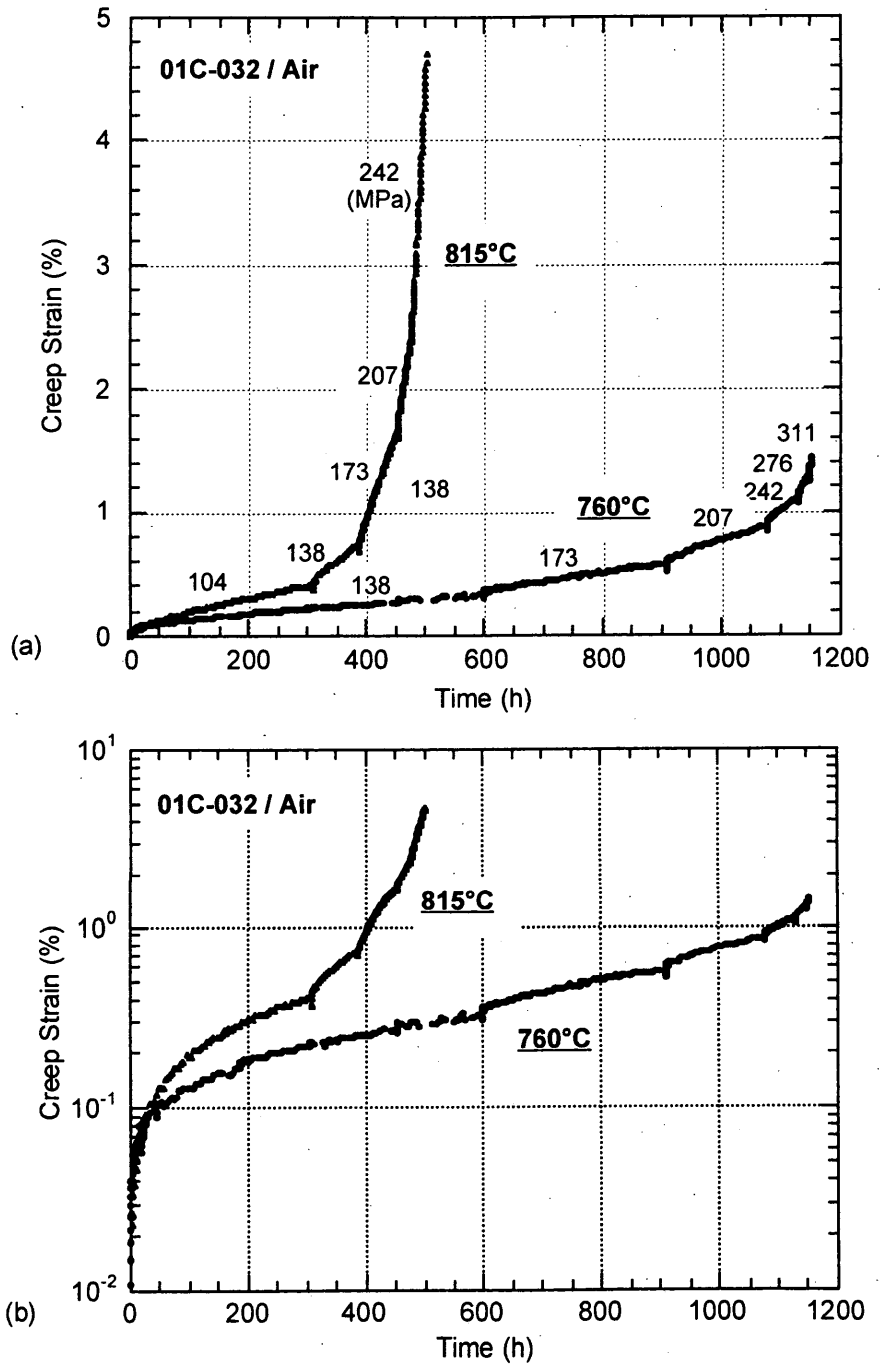

Fig. 4.6 Creep Curves at 760°C in stress-increase testing conditions

As expected, increase in test temperature from 760°C to 815°C enhanced creep strain substantially. It is also expected that at 815°C the rupture strain is greater and that the rupture time is much shorter as compared to those at 760°C. From the creep curves of all tested specimens, respective minimum creep rates were analyzed and plotted against respective stress values, as shown in Fig.4.7

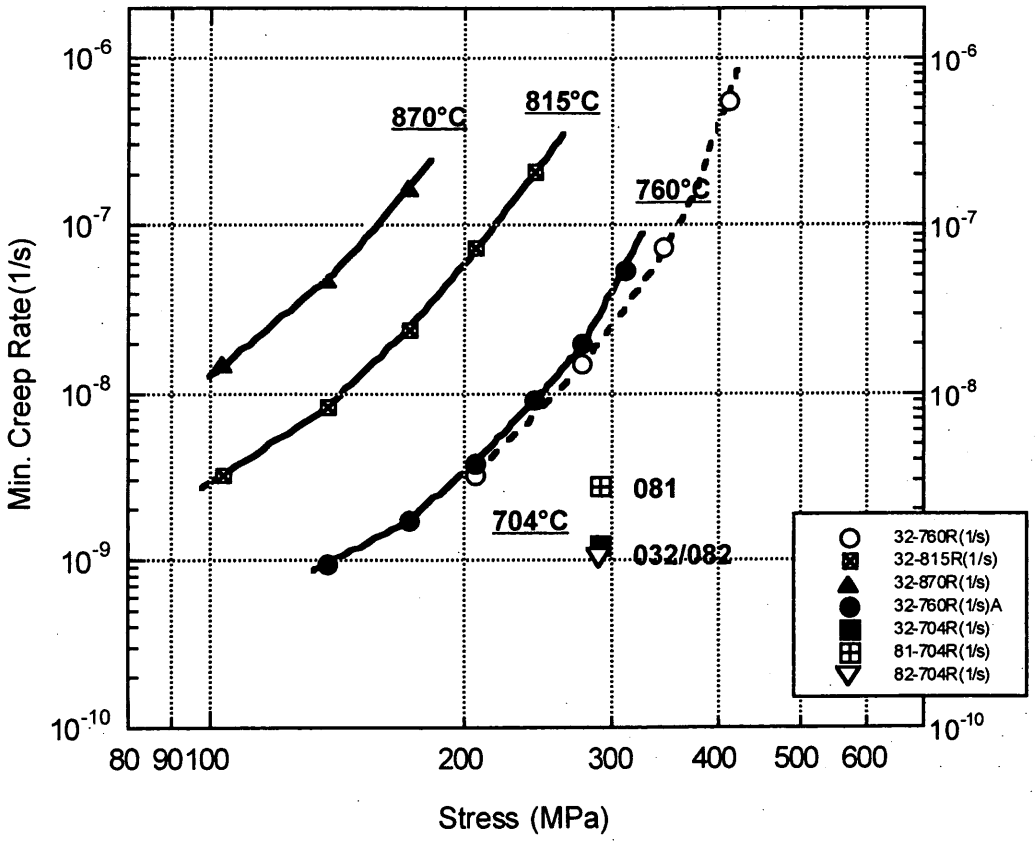

Fig. 4.7: Minimum creep rates as functions of temperature and applied stress for 01C fully-lamellar specimens in various aging conditions (032, 081 and 082)

Several important observations can be made from Fig. 4.7. 01C-032 specimens exhibit a exist constantly increasing n values (min. creep rate vs. stress in log scale) at all temperatures tested. The n values range between 2.7 and 8.5 at 760°C and between 3.3 and 6.8 at 815°C. Slightly lower n values were estimated for 870°C for a given stress level. This suggests that deformation by dislocation motion is important, especially, for high stress levels for all temperatures. Another interesting feature is that for a given applied stress, creep rate increases appear to be reduced with increasing temperature. At 704°C, both 01C-032 and 01C-082 specimens show identical minimum creep rates suggesting that the single-step aging (032) and two-step aging (082) may have resulted in carbide distributions

that may be effectively similar. As indicated earlier, the reasons for the greater creep resistance shown in 01C-082 material, as compared to 01C-081 material, are not clear. Extensive TEM observations and analysis may be needed.

5.0 Material Supply to GRC

Toward the end of the 2nd quarter of the contract period, plate samples of 01A-31, 01B-031and 01C-031 (see Table 4.1 and Fig. 4.1) were supplied to GRC. Dr. J. Daniel Whittenberger of GRC conducted compression testing on these materials and determined compressive behavior, including creep response, between 1000 and 1300 K in air at constant crosshead speeds ranging from 0.021 to 2.1 x 10^{-6} mm/s. Detailed results and discussion are described in Appendix A.

As discussed earlier, 032 heat treatments introduced fully-lamerllar structures in both 01B and 01C alloys (see Table 4.1), both having similar grain sizes around 120 μm. During the latter half of the contract period, six (6) tensile-creep specimens were machined from each of 01B-032 and 01C-032 samples. These specimens were provided to Dr. Whittenberger. In addition, four (4) tensile-creep specimens were machined from each of 01C-081 and 01C-082 materials (see table 4.1 and Fig. 4.2), and these eight (s) specimens were also provided to GRC toward the end of the contract. Testing of these specimens is outside of this contractual work, but is being carried out by Dr. Whittenberger.

6.0 Summary and Recommendations

Four different alloys, with the compositions formulated on the basis of alloy K5 (Ti-46.2Al-2Cr-3Nb-0.2B), were investigated for their microstructure evolution, aging responses, and tensile and creep behavior in fully lamellar (FL) microstructure forms. These alloys are listed below.

01A: Ti-47.0Al-1.7Cr-3.0Nb-0.20W-0.18B-0.23C-0.2Ox

01B: Ti-45.6Al-1.5Cr-3.1Nb-0.31W-0.15B-0.43C-0.19Ox

01C: Ti-45.7Al-1Cr-3.0Nb-0.30W-0.18B-0.40C-0.2Si-0.23Ox

01D: Ti-44.7Al-1.7Cr-3.0Nb-0.20W-0.20B-0.30C **(=K5A)**

As expected, the RT strengths mainly depended on the Al content, that is, 01D alloy fully showed the highest strength levels for a given cooling/aging combination and alloy 01A had the lowest level. Alloy 01D, on the other hand, showed the lowest tensile ductility. Alloy 01C FL showed the RT strength greater (by 30-50 MPa) than that of 01B FL, and tensile ductility comparable to that of 01BFL. Extensive aging experiments were conducted at 800°C, 900°C and 1000°C on FL alloy materials produced by respective annealing of (alpha-anneal for 2h, furnace cool to 1200°C and then air cool). Aging reduced the volume fraction of alpha-2 plates, which resulted in the breaking up of alpha-2 plates and the formation of carbides and also silicides. This process resulted in the reduction of the RT tensile strengths for all alloys except for the early stages of aging on 01D alloy FL. However, it was analyzed that aging improves the creep resistance, as measured for 01B and 01C material at 704°C, 760°, and 815°C. It is judged that among the four alloys, alloy 01C in appropriately aged FL forms appears to show the best combination of tensile and creep properties. It is recommended that future alloy design may have to be based on the 01C composition.

It was fundamentally understood that as-formed lamellar material contains almost all carbon dissolved in the alpha-2 plates, and upon aging the alpha-2 volume fraction decreases and carbon is segregated into carbides. The resulting lamellar microstructure is now alternating layers of gamma lath and particle array. These particle arrays apparently interact strongly with dislocations moving in the easy orientations (parallel to the arrays). Both promising strength levels and drastically enhanced creep resistance could be achieved when Al and C contents are properly set and optimum two-step aging treatments are formulated. Combinations of Al and C contents and aging conditions will pay a critical role in improvement of creep resistance. Optimizing/controlling the distribution of carbides is possible through two-step aging process and needs to be further investigated.

Appendix A. Elevated Temperature Deformation Behavior in Compression

Dr. J. Daniel Whittenberger
GRC

Materials

01A-031, 01B-031 and 01C-031: All alloys were given a 1000 °C, 3h, FC stress relief; then 1360 °C, 2h; FC to 1200 °C, AC anneal and finally aged at 900 °C for 48 h (Table 4.1). This resulted in a nearly full lamellar structure in 01A and FL microstructures in 01B and 01C. I do not have an exact description of the microstructure in terms of the grain size, lath spacing prior to the aging treatment, nor carbide/silicide/boride precipitate distribution after aging.

Compressive Test Procedures

Four mm diameter by 8 mm long compression test specimens were electro discharge machined {EDM'ed} from each of the forged + heat treated alloys, where the long axis of the samples was perpendicular to the forging direction. Elevated temperature compressive behavior between 1000 and 1300 K in air was determined both under constant velocity and constant load creep conditions on as-EDM'ed samples. Load - time charts from a universal test machine operating at constant crosshead speeds ranging from 0.021 to 2.1 x 10^{-6} mm/s were converted to true stresses, strains, and strain rates via the offset method and the assumption of conservation of volume. Creep response of the specimens was measured by super linear variable displacement transducers which determined the relative positions of ceramic push bars applying a constant load to the specimen. During testing, the contraction readings were stored in a data acquisition system as a function of time. Most of the creep tests were subjected to multiple constant load conditions, where the load was increased once a prolonged period of steady state creep had been obtained. Following completion of each creep experiment, the results were normalized with respect to the final specimen length and converted into true stress and strains by also assuming volume conservation.

Results and Discussion

The true compressive stress – strain curves from constant velocity testing are presented for nearly fully lamellar alloy 01A-031 {01A} and fully lamellar alloys 01B-031 {01B} and 01C-031 {01C} in Figs. 1-3, respectively, as functions of temperature and nominal imposed strain rate. At 1000 K all three alloys (Parts (a) of Figs 1-3) exhibited continuous strain hardening at the fastest imposed strain rate (~2.2 x 10^{-3} s^{-1}). The tendency for continuous work hardening at 1000 K, however, lessened as the imposed strain rate decreased such that the alloys only exhibited a small amount of strain hardening followed by continued deformation at a more or less constant stress at the slowest strain rate (~2.2 x 10^{-7} s^{-1}). This latter pattern also basically describes the compressive stress – strain response of all three alloys at 1100 K (Parts (b) of Figs. 1-3), 1200 K (Parts (c) of Figs. 1-3) and 1300 K (Parts (d) of Figs. 2 & 3) as a function of imposed deformation rate.

True compressive constant load creep curves for the three TiAl alloys are given in Figs. 4-6 as function of engineering stress and temperature. In all cases the alloys exhibited normal creep behavior upon initial loading, where the strain rate decreased with increasing time during the transient creep stage until an apparent steady state regime with a constant strain rate was reached. For the multi-load experiments, the subsequent stress increases produced two patterns: (1) an almost immediate transition to steady state when the higher stress was applied {Fig. 4, 1000 K – 286 MPa and 1100 K – 79.5 MPa; Fig. 5(a), 1100 K – 172 MPa; Fig. 5(b), 1200 K – 76 MPa; and Fig. 6(a), 1100 K – 197MPa} or (2) a normal creep response with definite transient and steady state regimes {Fig. 4, 1000 K – 231 MPa; Fig. 5(a), 1000 K – 323 & 395 MPa; and Fig. 6(a), 1000 K – 390 MPa after the power shut down}.

True compressive flow stress (σ) - strain rate ($\dot{\varepsilon}$)- temperature (T) results for all three alloys are presented in Figs. 7-9. In these figures the flow stresses evaluated from constant velocity testing {open symbols} are represented by the stress at 3 % strain from the stress - strain curves (Figs. 1-3), while the flow stresses from creep testing {solid symbols} are the average true stress calculated over each steady state regimes (Figs. 4-6). The semi-logarithmic plots of the data in Parts (a) for Figs. 7-9 indicate that there is a linear relationship between logarithm strain rate and stress over the majority of the testing range at 1000 and 1100 K, but this type of behavior is not maintained at the higher test temperatures. Log – log plots of the flow stress - strain rate – temperature results (Parts (b) of Figs. 7-9), on the other hand, linearize most of the higher temperature data as well as significant portions of the slower strain rate values at 1000 and 1100 K. As indicated by the curves in Figs. 7(b), 8(b) and 9(b), the creep properties of three alloys could be described by a temperature compensated power law equation

$$\dot{\varepsilon} = A_o \sigma^n \exp(-Q/(RT)) \qquad (1)$$

where the strain rate is in s^{-1} A_o is a constant, the flow stress is in MPa, Q is the activation energy for deformation, R is the universal gas constant and T is the temperature. This fit was accomplished by multiple linear regression techniques, and the resultant values for A_o, n, Q and the standard deviations for the stress exponent (δn) and activation energy (δ_Q) as well as the coefficients of determination (R_d^2) are given in Table 1. Based on visual inspection of the lines in Figs. 7(b), 8(b) and 9(b) and the coefficients of determination (Table 1), a temperature compensated power law describes the experimental data for each material well.

Because the n and Q values in Table 1 are essentially identical for all three alloys, elevated temperature slow plastic deformation of these materials appears to take place by the same mechanism. To this end, dummy variables were used in a regression analysis to force the same n and Q values but different A_o's for each material. The results of this fitting are also presented in Table 1, where the A_o for alloy 01B is about 5 % of that for alloy 01A (131.2 vs. 2810) and the A_o for alloy 01C is 65 % of that for 01B (85.8 vs. 131.2). This approach directly indicates that the creep resistance of alloy 01A is much less than either alloys 01B or 01C, and, in turn, alloy 01C is slightly stronger than alloy 01B.

Table 1. Temperature Compensated Power Law Deformation parameters for TiAl-based Alloys

Alloy	A_o, s^{-1}	n	Q, kJ/mol	δ_n	δ_Q, kJ/mol	R_d^2
01A	3593	4.93	430.1	0.22	21.3	0.978
01B	185.2	4.95	432.5	0.16	11.7	0.991
01C	55.8	4.85	419.7	0.19	14.2	0.984
01A 01B 01C	2810 131.2 85.8	4.91	426.9	0.11	8.5	0.984

Figure 10 compares the flow stress – strain rate –temperature properties of alloy 01C tested in compression (Fig. 9) and under multi-stress tensile conditions. This tensile data was determined on samples essentially given the same heat treatment as the compression specimens with the exception that the tensile samples were annealed at a slightly higher temperature (1370 °C for 2 h). Visually, the tensile and compressive data (Fig. 10) appear to be in good agreement. This hypothesis was tested by multi-linear regression analysis using a dummy variable in combination with eqn (1) over the valid temperature compensated power law compression data regime (Fig. 9(b)) and all the tensile results shown in Fig. 10. This test indicated that there was no difference between the results generated under either compression or tensile conditions, and the pooled data could be described by

$$\dot{\varepsilon} = 35.3\ \sigma^{4.93} \exp(-419.6/(RT)), \qquad (2)$$

where the R_d^2 for the fit is 0.981 and the standard deviations for the stress exponent and activation energy are 0.16 and 11.9 kJ/mol, respectively.

Recently Zhang and Deevi [W.J. Zhang and S.C. Deevi, Structural Intermetallics 2001, (eds. K.J. Hemker, D.M. Dimiduk, H. Clemens. R. Darolia, H. Inui, J.M Larsen, S.K. Sikka, M. Thomas and J.D. Whittenberger) TMS, Warrendale, PA, 2001 pp.699-708.] have reviewed the literature to determine the rate limiting factors for creep in TiAl and basically concluded that fine lamellar spacing produces the strongest alloys, at least for simple compositions. Furthermore the slower strain rate creep resistance can be increased by the addition of (C,N,Si) and B and W; all of which exist in the current three alloys. While Zhang and Deevi did not quantify the effects of these alloy elements, they did develop an equation to describe the minimum creep rate of fine lamellar spacing (~0.1 μm) TiAl alloys, where

$$\dot{\varepsilon} = 2.17 \times 10^9 \sinh(\sigma/62) \exp(-375./(RT)). \qquad (3)$$

The predictions of eqn (3) are compared to the observed behavior of alloy 01C between 1000 and 1300 K in Fig. 11. This comparison indicates that O1C is nearly as strong as fine lamellar spacing TiAl at faster deformation rates and/or at lower temperatures; but at higher temperatures or slower strain rates, the 01C displays much better properties.

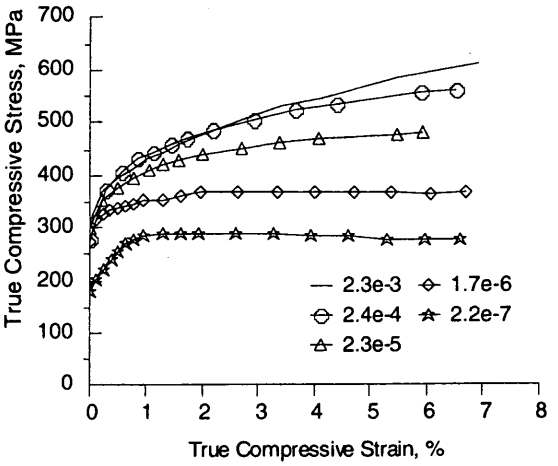

Figure 1(a). True compressive stress – strain curves for nearly fully lamellar alloy 01A tested in air at 1000 K as a function of nominal strain rate (s^{-1}).

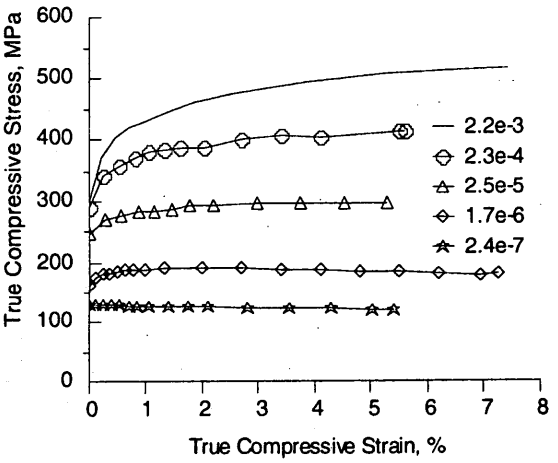

Figure 1(b). True compressive stress – strain curves for nearly fully lamellar alloy 01A tested in air at 1100 K as a function of nominal strain rate (s^{-1}).

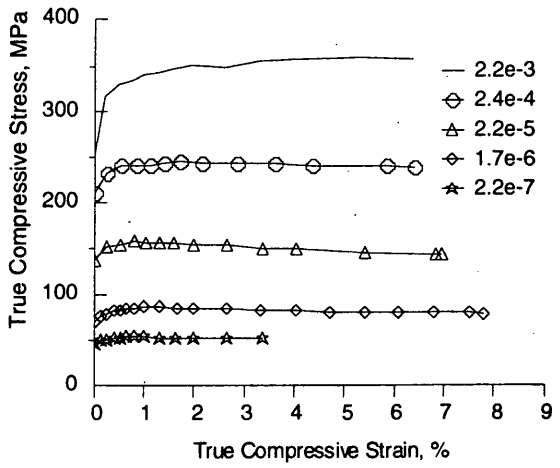

Figure 1(c). True compressive stress – strain curves for nearly fully lamellar alloy 01A tested in air at 1200 K as a function of nominal strain rate (s^{-1}).

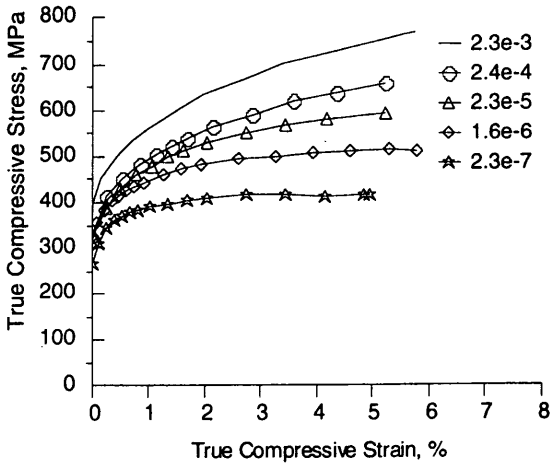

Fig. 2(a). True compressive stress – strain curves for fully lamellar alloy 01B tested in air at 1000 K as a function of nominal strain rate (s^{-1}).

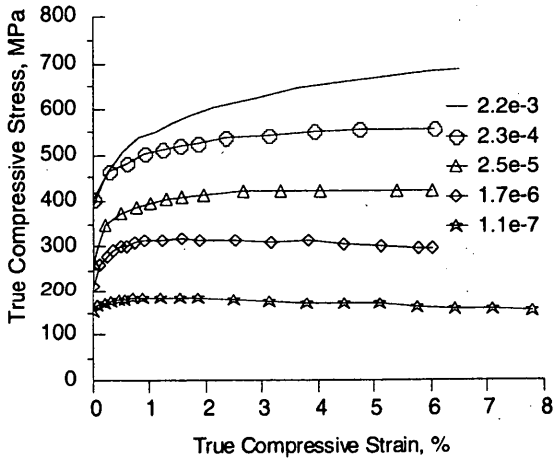

Fig. 2(b). True compressive stress – strain curves for fully lamellar alloy 01B tested in air at 1100 K as a function of nominal strain rate (s^{-1}).

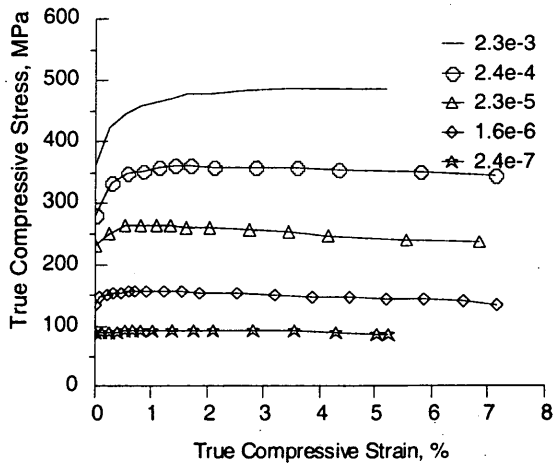

Fig. 2(c). True compressive stress – strain curves for fully lamellar alloy 01B tested in air at 1200 K as a function of nominal strain rate (s^{-1}).

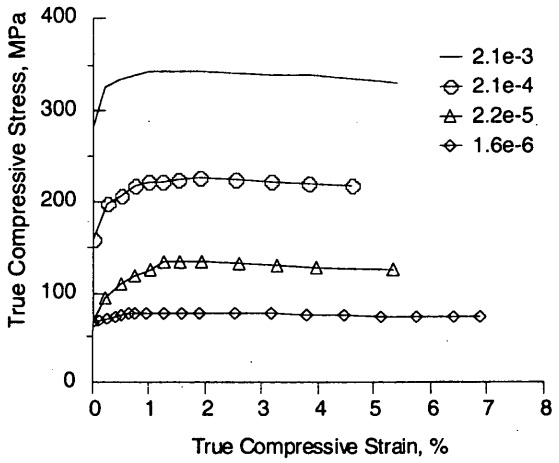

Fig. 2(d). True compressive stress – strain curves for fully lamellar alloy 01B tested in air at 1300 K as a function of nominal strain rate (s^{-1}).

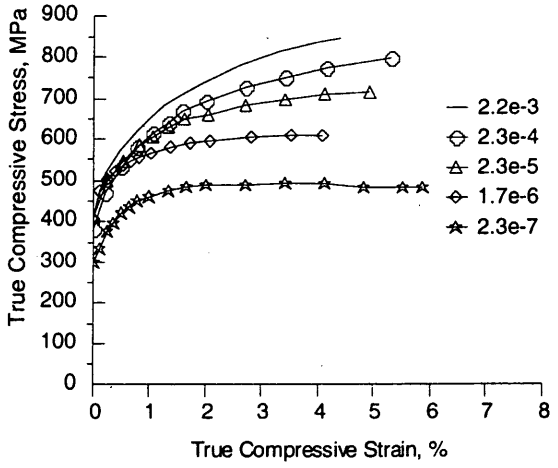

Fig. 3(a). True compressive stress – strain curves for fully lamellar alloy 01C tested in air at 1000 K as a function of nominal strain rate (s^{-1}).

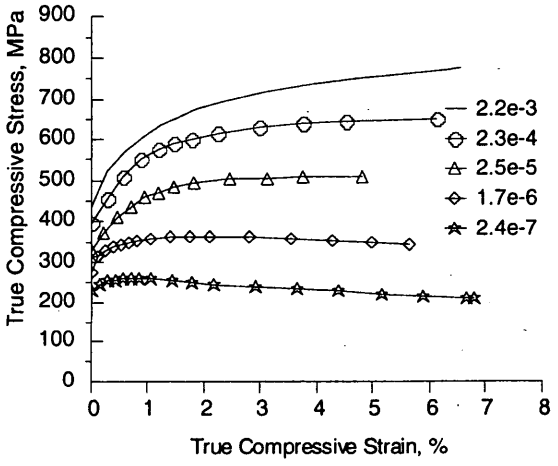

Fig. 3(b). True compressive stress – strain curves for fully lamellar alloy 01C tested in air at 1100 K as a function of nominal strain rate (s^{-1}).

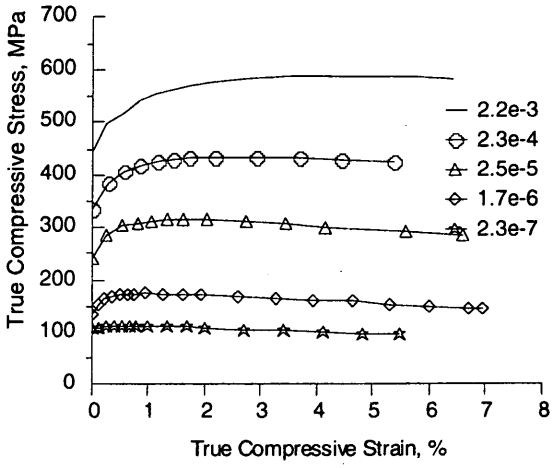

Fig. 3(c). True compressive stress – strain curves for fully lamellar alloy 01C tested in air at 1200 K as a function of nominal strain rate (s^{-1}).

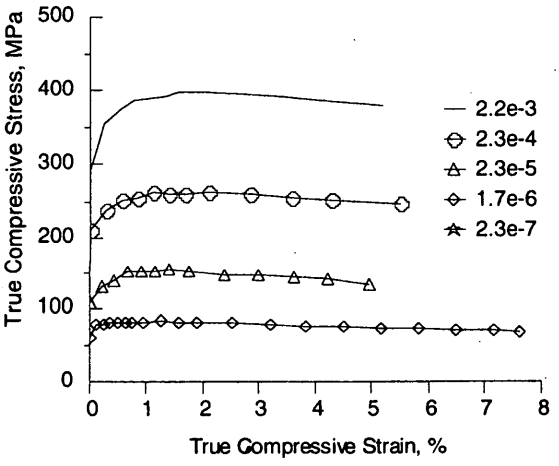

Fig. 3(d). True compressive stress – strain curves for fully lamellar alloy 01C tested in air at 1300 K as a function of nominal strain rate (s^{-1}).

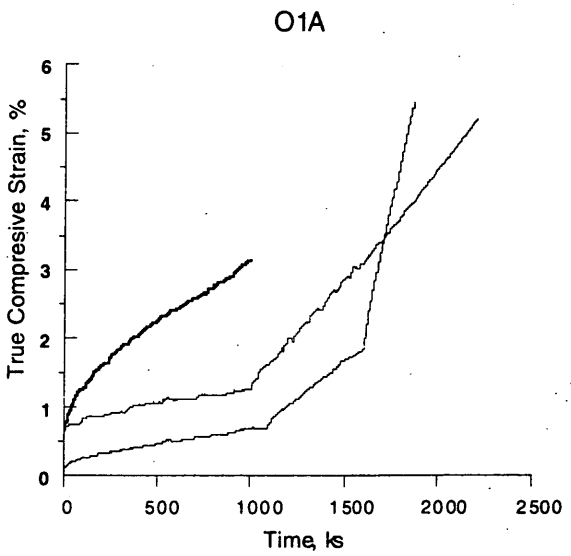

Figure 4. True compressive creep curves for nearly fully lamellar alloy 01A tested at 1000 K and engineering stresses 175, 231 & 286 MPa (thin curve); at 1100 K and engineering stress of 50 & 79.5 MPa (medium curve); and 1200 K and an engineering stress of 30 MPa (thick curve).

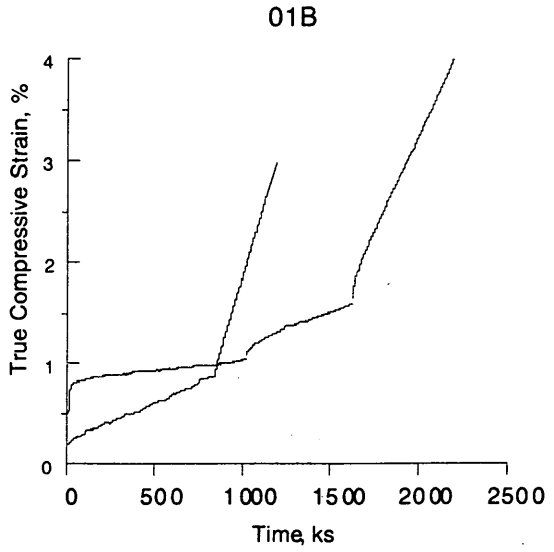

Figure 5(a). True compressive creep curves for fully lamellar alloy 01B tested at 1000 K and engineering stresses of 250, 323 & 395 MPa (thin curve); and at 1100 K and engineering stresses of 100 & 172 MPa (medium curve).

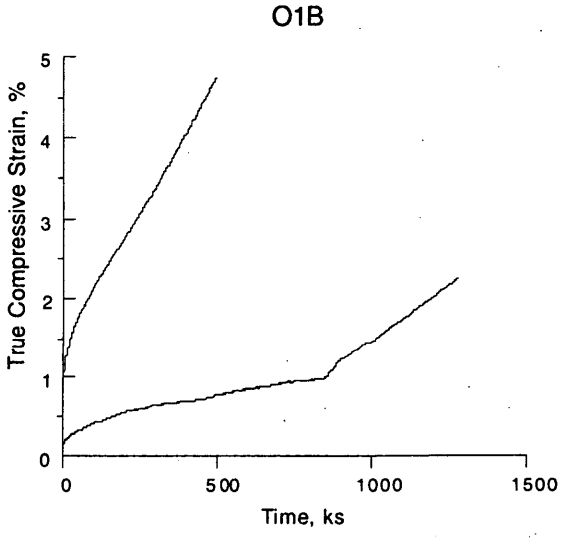

Figure 5 (b). True compressive creep curves for fully lamellar alloy 01C at 1200 K and engineering stresses of 50 & 76 MPa (thin curve); and at 1300 K and an engineering stress of 40 MPa (medium curve).

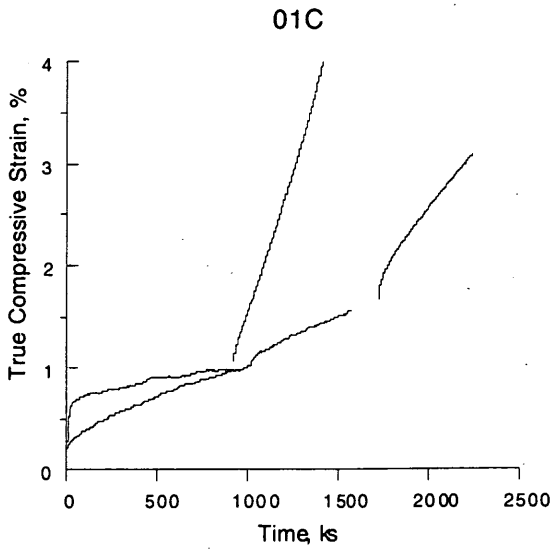

Figure 6(a). True compressive creep curves for fully lamellar alloy 01C tested at 1000 K and engineering stresses of 300 and 390 followed by 390 MPa again after a power shut down (thin curve); and at 1100 K and engineering stresses of 125 & 197 MPa (medium curve).

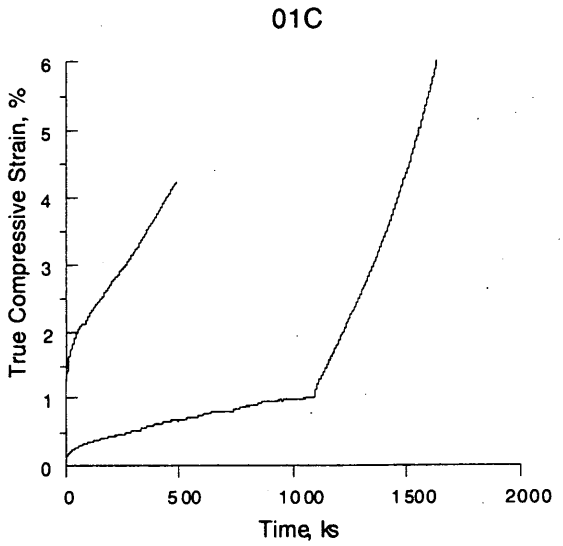

Figure 6 (b). True compressive creep curves for fully lamellar alloy 01C at 1200 K and engineering stresses of 50 & 93 MPa (thin curve); and at 1300 K and an engineering stress of 40 MPa (medium curve).

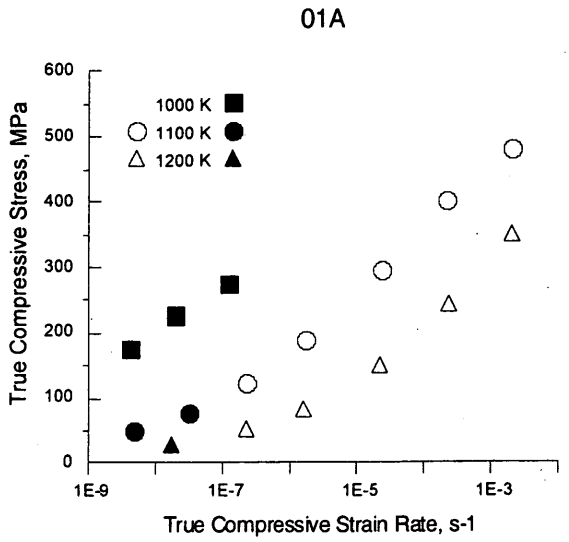

Figure 7 (a). Semi- logarithmic presentation of the true compressive flow stress – strain rate – temperature behavior of nearlly fully lamellar alloy 01A. The open symbols represent constant velocity test data, while the filled symbols represent constant load creep test results.

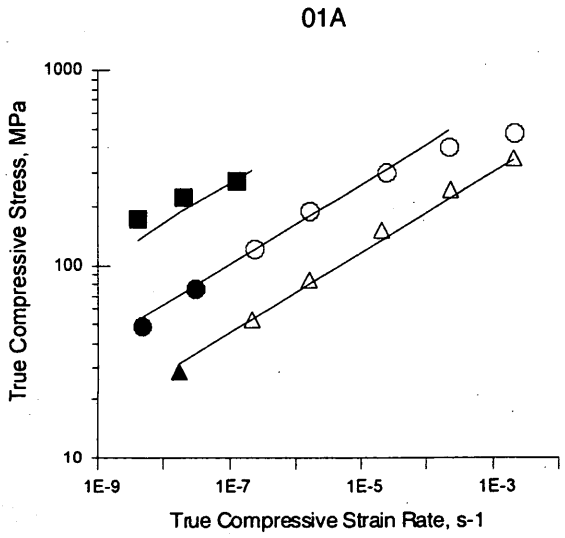

Figure 7 (b). Logarithmic presentation of the true compressive flow stress – strain rate – temperature behavior of nearlly fully lamellar alloy 01A. The open symbols represent constant velocity test data, while the filled symbols represent constant load creep test results.

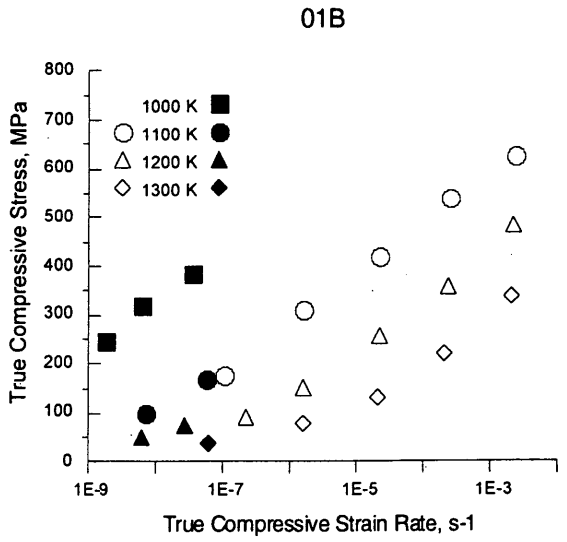

Figure 8 (a). Semi- logarithmic presentation of the true compressive flow stress – strain rate – temperature behavior of fully lamellar alloy 01B. The open symbols represent constant velocity test data, while the filled symbols represent constant load creep test results.

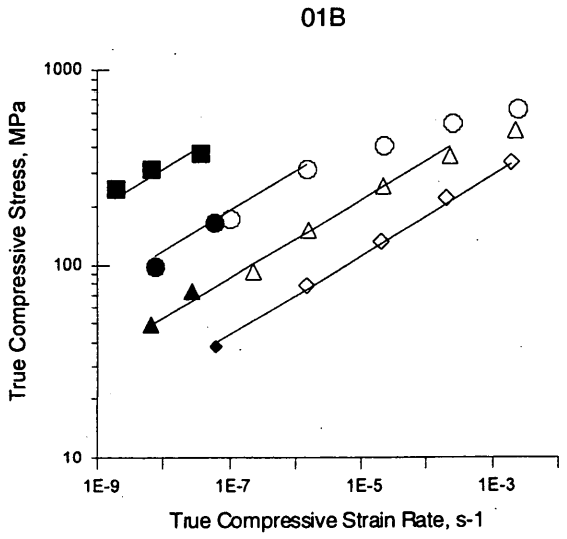

Figure 8 (b). Logarithmic presentation of the true compressive flow stress – strain rate – temperature behavior of fully lamellar alloy 01B. The open symbols represent constant velocity test data, while the filled symbols represent constant load creep test results.

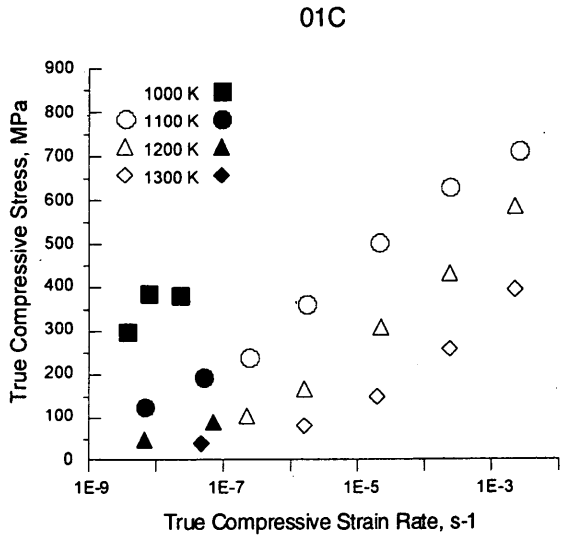

Figure 9 (a). Semi- logarithmic presentation of the true compressive flow stress – strain rate – temperature behavior of fully lamellar alloy 01C. The open symbols represent constant velocity test data, while the filled symbols represent constant load creep test results.

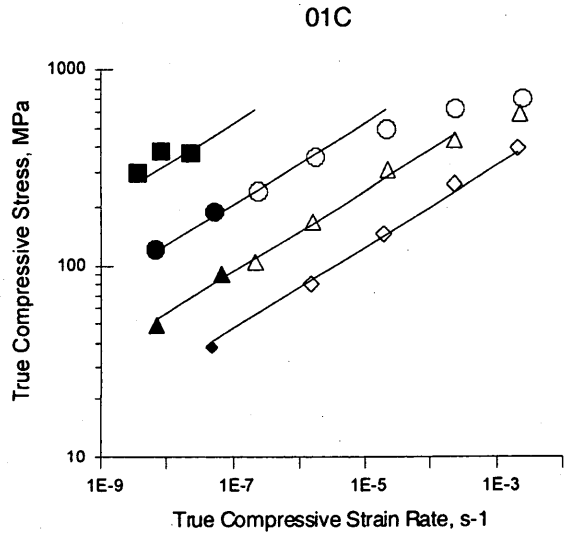

Figure 9 (b). Logarithmic presentation of the true compressive flow stress – strain rate – temperature behavior of fully lamellar alloy 01C. The open symbols represent constant velocity test data, while the filled symbols represent constant load creep test results.

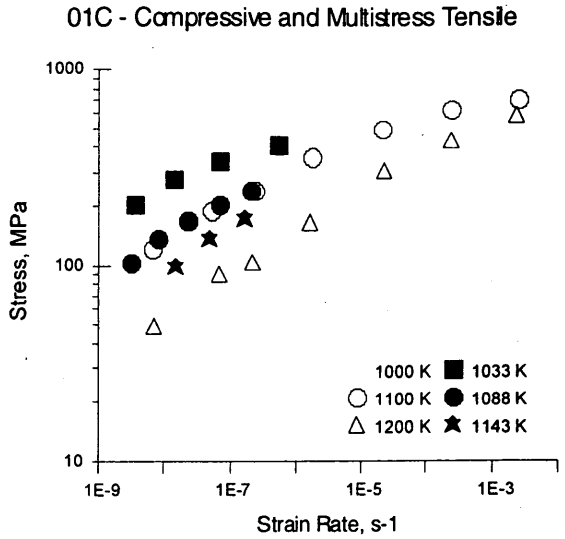

Figure 10. Logarithmic presentation of the flow stress – strain rate – temperature behavior of fully lamellar alloy 01C tested in compression (open symbols) and in multi-stress tension (solid symbols) between 1000 and 1200 K.

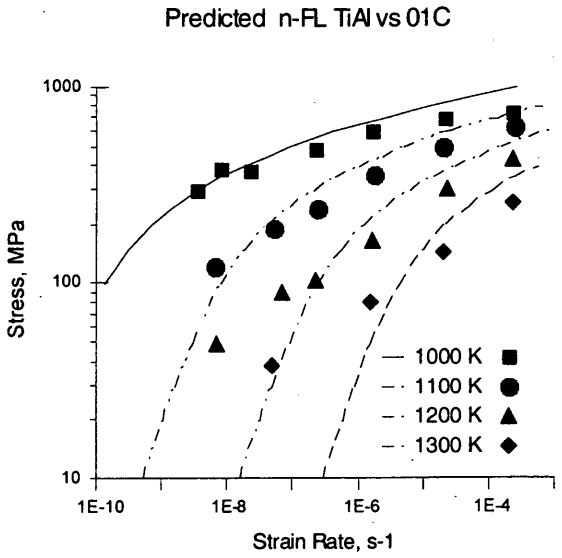

Figure 11. A comparison of the compressive flow stress – strain rate – temperature properties for fully lamellar alloy 01C (solid symbols) to Zhang and Deevi's predicted behavior for fine lamellar spacing TiAl.

REPORT DOCUMENTATION PAGE

Form Approved
OMB No. 0704-0188

1. REPORT DATE *(DD-MM-YYYY)*	2. REPORT TYPE	3. DATES COVERED *(From - To)*
11 June 2002	Final Report	3 Feb 2001 - 31 May 2002

4. TITLE AND SUBTITLE
Designing Gamma TiA1 Alloys (K5 Based for Use at 840 C and Above)

5a. CONTRACT NUMBER
C-7076-N

5b. GRANT NUMBER

5c. PROGRAM ELEMENT NUMBER

6. AUTHOR(S)
Dr. Young-Won Kim, Principal Investigator
UES, Inc.
4401 Dayton-Xenia Road
Dayton, OH 45432

5d. PROJECT NUMBER
UES Project No. 707

5e. TASK NUMBER

5f. WORK UNIT NUMBER

7. PERFORMING ORGANIZATION NAME(S) AND ADDRESS(ES)
UES, Inc.
4401, Dayton-Xenia Road
Dayton, OH 45432

8. PERFORMING ORGANIZATION REPORT NUMBER

9. SPONSORING/MONITORING AGENCY NAME(S) AND ADDRESS(ES)
NASA Glenn Research Center
21000 Brookpark Road
Cleveland, OH 44135-3191

10. SPONSOR/MONITOR'S ACRONYM(S)
M/S 500-306

11. SPONSOR/MONITOR'S REPORT NUMBER(S)

12. DISTRIBUTION/AVAILABILITY STATEMENT

13. SUPPLEMENTARY NOTES

14. ABSTRACT

The objective of this program was to investigate how carbon additions and A1 content variation affects RT tensile properties and creep performance in gamma TiA1 alloys. On the basis of the results from the work under GRC Contract C-7076-K, four alloys were selected within the composition range of Ti-(44.7-47.0) Al-(1.0-1.7)Cr-3.0Nb-0.2W-0.2B-(0.23-0.43)C-(0, 0.2)Si. Through extensive annealing/aging experiments, detailed observations of microstructure evolution, property measurements and analyses, comprehensive understanding was made in the carbide formation process. It was found that creep properties depend on the distribution of carbide particles, which is controlled not only by the aging process but also the amount ratio fo A1 and carbon. From the results and analysis, new creep-resistant alloy compositions are suggested for further development.

15. SUBJECT TERMS
Gamma TiA1 Alloys, Creeep Properties, Carbide Formation Process

16. SECURITY CLASSIFICATION OF:			17. LIMITATION OF ABSTRACT	18. NUMBER OF PAGES	19a. NAME OF RESPONSIBLE PERSON
a. REPORT	b. ABSTRACT	c. THIS PAGE			Dr. Young-Won Kim
UNCLAS	UNCLAS	UNCLAS	SAR	67	19b. TELEPHONE NUMBER *(Include area code)* 937/255-1321